FINITE ELEMENT ANALYSIS OF MULTIPASS EFFECTS OF VEHICLES ON SOIL COMPACTION

by

David G. Pollock, Jr.

thesis submitted to the Faculty of the

Virginia Polytechnic Institute and State University

in partial fulfillment of the requirements for the degree of

MASTER OF SCIENCE

in

Agricultural Engineering

APPROVED:

Dr. John V. Perumpral

Dr. T. Kuppusamy

Dr. John Cundiff

February, 1984
Blacksburg, Virginia

FINITE ELEMENT ANALYSIS OF MULTIPASS EFFECTS OF VEHICLES ON SOIL COMPACTION

by

David G. Pollock, Jr.

(ABSTRACT)

A computer program based on the finite element procedure was modified to analyze the multipass effect of rubber-tired vehicles on soil compaction.

The wheel-soil interaction was modeled as an axisymmetric problem by approximating the elliptical wheel-soil contact area with an equivalent circular area. A hyperbolic stress-strain relationship was used to model the nonlinear material characteristics of the soil. The boundary load conditions were based on contact area and contact pressure data for a standard tire.

The finite element program developed was verified by conducting a linear elastic analysis of a circular flexible footing problem and comparing the results with closed form solution. The results of the finite element analysis agreed well with the closed form solution.

The effects of soil type, wheel-soil contact area, and multiple wheel loading on soil compaction were analyzed. The results of the analyses provided information on soil

displacement, stress distribution, and volumetric strain. Residual volumetric strain contours, developed after each loading and unloading cycle (simulating the passage of a wheel), showed zones of maximum compaction and the propogation of compaction zones as a function of the number of wheel loadings. A major portion (80% - 90%) of the total residual volumetric strain was found to occur during the first wheel pass. The rate of increase in volumetric strain dropped noticeably as the number of passes increased. As expected, results of the analysis show that for a given vehicle weight, the use of large tires minimizes the degree of compaction.

DO YOU NOT KNOW? HAVE YOU NOT HEARD?

The Lord is the everlasting God, the Creator of the ends of the earth. He will not grow tired or weary, and His understanding no one can fathom. He gives strength to the weary and increases the power of the weak. Even youths grow tired and weary, and young men stumble and fall; but those who hope in the Lord will renew their strength. They will soar on wings like eagles; they will run and not grow weary, they will walk and not be faint.

Isaiah 40:28-31

ACKNOWLEDGEMENTS

The author would like to express deep appreciation to his committee chairman, Dr. John V. Perumpral, for his support and guidance throughout the graduate program. He has been an outstanding example of professionalism and a true friend to the author. Appreciation must also be expressed to Dr. T Kuppusami for his guidance in employing the finite element method and for serving as a committee member. Special thanks to Dr John Cundiff for his prayers and support while serving as a committee member. The author would like to express appreciation to Deere and Company for the financial support of this project.

The author's deepest appreciation is extended to his parents, Mr. and Mrs. David G. Pollock, Sr., for their selfless love and support throughout his college career. Through their understanding, guidance, and exemplary lives they motivated the author to accomplish his goal and taught him the key to true success --- that God must be given first place in one's heart and in one's life. Thanks is also expressed to the author's grandmother, Mrs. E. N. Dodge, for her faithful prayers and loving encouragement. The author's appreciation extends to his sisters and brothers-in-law, Mr. and Mrs. Mike Edwards and Mr. and Mrs. Doug Hedrick, for their prayers and support.

Finally, appreciation is extended to Ms. Karin Buchanon for her assistance in preparing graphical figures for the text, and to Mr. and Mrs. Ed Beaver, Ms. Lynn Beaver, and the author's mother and grandmother for their assistance in editing and proofreading the text.

TABLE OF CONTENTS

LIST OF TABLES

LIST OF FIGURES

Chapter I

INTRODUCTION

Soil compaction may be defined as the decrease in volume that a soil experiences under an applied load. It is commonly expressed as a change in soil porosity or bulk density. The applied forces may include man-induced forces or natural forces such as freezing and thawing, rainfall, and root growth. Forces acting on soil prompt a decrease in volume and pore space through the rearrangement of soil particles. In most civil engineering applications soil compaction is considered a desirable feature because it yields increased soil strength. However, in agriculture it is not desired because the reduction in soil pore space can result in decreased water storage capacity, decreased hydraulic conductivity, high root impedance, and restricted flow of nutrients within the soil. These effects can ultimately cause substantial increases in runoff and soil erosion, and decreased crop yield.

Traffic of heavy equipment is regarded as the primary cause of soil compaction encountered in agriculture. Multiple passes of heavy machines have a cumulative effect, often causing the formation of a hardpan within the soil. The hardpan may restrict water transmission and root

penetration, creating long-term effects on crop productivity. These problems may become severe in areas where minimum tillage or no tillage practices are employed on a continual basis for raising crops.

An ability to analyze the soil compaction process is necessary to minimize the harmful effects associated with soil compaction. An understanding of the mechanics of compaction will enable soil scientists and engineers to predict how, when, and where a hardpan may develop in a particular soil profile under given loading conditions.

Many field and laboratory studies have been conducted to better understand the soil compaction process. Although valuable, these methods are generally labor intensive, time consuming, and expensive. These problems can perhaps be avoided if a computer model capable of simulating the soil compaction process is available. Such a model, however, cannot be considered a full replacement for experimental procedures. Rather, it can be used effectively to better understand the mechanics of soil compaction and the factors affecting it. Therefore, the overall objective of this study is to develop a generalized computer model which can be used to study the soil compaction process, and the effect of multiple vehicle passes on soil compaction.

Chapter II

OBJECTIVES

The specific objectives of this study are:

1. To develop a finite element model to predict the soil compaction resulting from vehicle traffic.
2. To predict the effect of multiple passes of a rubber tired vehicle on soil compaction and stress distribution.
3. To determine the effect of soil type on stress distribution and soil compaction resulting from vehicle traffic.
4. To predict the effect of tire size on soil compaction and stress distribution.

Chapter III

LITERATURE REVIEW

Soil compaction results from the interaction of a number of factors such as magnitude of surface loading, area under load, properties of the soil, moisture content of the soil, and stress history of the soil. A complete understanding of the soil compaction process requires the identification of the factors affecting soil compaction and their interrelationships. Only then will it be possible to model the soil compaction process. During the past twenty-five years researchers have identified many of these factors and attempted to describe their influence on soil compaction.

3.1 FACTORS INFLUENCING COMPACTION

Soehne (1958) concluded from a laboratory study that soil compaction depends on the size and shape (rectangular, elliptical, circular) of the contact area through which the surface load is applied. He also found that the distribution of pressure (uniform or parabolic) over the contact area influences the resulting degree of compaction. Jaafari and Bowen (1980) found that total vehicle weight and draft force on the tractor influence soil compaction.

The importance of soil type and moisture content on the degree of compaction has been observed by many researchers (Soehne, 1958; Gill and Reaves, 1956; Negi, et al., 1981; King, 1979). There exists a critical moisture level for attaining maximum compaction in each type of soil. When the moisture content of any given soil approaches this critical moisture level, the passage of even a relatively light vehicle may result in considerable soil compaction. In a similar study, Minaei (1983) observed that a 3% increase in moisture content resulted in a 144% increase in bulk density due to nine passes of a rubber-tired vehicle.

Bodman and Rubin (1948) were the first to suggest that the application of shear stress also causes soil compaction. Until then it was believed that soil compaction was the result of normal stress alone. Subsequent studies by Harris, et al. (1964) and Raghavan, et al. (1977) have also shown the influence of shear stress on compaction. Raghavan, et al. observed that shear stress caused by wheel slip may increase the soil bulk density by as much as 45%. Raghavan and McKyes (1978) observed that wheel slip ranging from 0% to 30% caused an increase in soil density, while slips of greater than 30% resulted in the formation of deep ruts as soil was thrown behind the tractive device. Recent studies by Bergmann (1979) and Stafford and Mattos (1981)

suggest that vehicle speed is another factor which can influence the soil compaction process. Stafford and Mattos theorized that as vehicle speed increases, slip decreases resulting in less compaction of the soil.

Bailey (1971) proposed that the stress history of a soil can also influence the degree of compaction it experiences. Recent experimental studies support Bailey's theory and note a strong correlation between the number of vehicle passes and the resulting soil compaction (Bergmann, 1979; Taylor, et al.,1979; Froehlich, et al., 1980; Jaafari and Bowen, 1980; Minaei, 1983). Froehlich, et al. (1980) noted that 60% - 90% of the compaction in forest soils of the Tahoe National Forest occurred during the first six passes of a vehicle. Similarly, Minaei (1983) noted that the first five passes of a vehicle accounted for the majority of compaction observed in a soil of southwestern Virginia. These studies suggest that after repeated loadings, a soil will reach a condition where additional vehicle traffic will result in virtually no change in bulk density.

3.2 STRESS DISTRIBUTION DUE TO BOUNDARY LOADS

In 1885 J. V. Boussinesq proposed a theoretical analysis of stress distribution due to applied loads. Boussinesq considered the stress distribution resulting from a point load acting on a semi-infinite, homogeneous, isotropic mass. Using the mathematical basis of the theory of elasticity, equations to predict the vertical stress (σ_z), radial stress (σ_r), tangential stress (σ_θ), shear stress (τ), radial displacement (δ_r), and vertical displacement (δ_z) at any point within the semi-infinite medium due to the applied load were developed. Because of the simplifying assumptions of homogeneity and linear elastic response of the soil, these equations fail to give accurate predictions of stress within a soil mass. However, they do serve to provide rough estimates of the stresses resulting from a boundary load (Jumikis, 1962).

In 1934, O. K. Froehlich modified the Boussinesq equations by adding a concentration factor to account for soil conditions. The concentration factor for a particular field setting was a subjective choice based on the observer's previous experience and his analysis of soil properties (Soehne, 1958). Taylor, et al. (1978) reported satisfactory prediction of stress distribution in a homogeneous soil using Froehlich's equations. However, they

noted that his method fails to predict the stress distribution accurately in a soil containing a hardpan beneath the surface. They also noted that neither Boussinesq nor Froehlich proposed an analytical procedure for predicting the bulk density of soil from a known stress distribution.

Soehne (1958) employed Froehlich's equation to obtain the stress distribution due to a surface load distributed over a finite area. The total loaded area was divided into a number of smaller areas, each with a portion of the total load acting at its centroid. He then integrated over the total area to sum the effects of this assemblage of point loads and to determine the resulting stress distribution.

3.3 SOIL COMPACTION DUE TO BOUNDARY LOADS

Soehne (1958) proposed the following relationship between soil porosity and the pressure at a point in the soil:

$$n = (-A) \log(p) + C \qquad [1]$$

where n = soil porosity

p = pressure

A, C = soil constants determined from static compaction tests

Soehne's work provided both a means for quantitatively describing soil compaction and a more realistic method for simulating a tire loading. The accuracy of these predictions is limited due to the assumption of linear elastic soil response and a failure to consider boundary effects at the outer edges of the loaded area.

VandenBerg, et al. (1958) proposed that soil bulk density depends solely on mean normal stress (σ_m). Continuum mechanics theory formed the basis of their analysis. It states that the spherical stress tensor is responsible for the change in volume while the deviatoric stress tensor produces a change in shape. They concluded that a knowledge of the mean normal stress distribution in a mass of soil would be sufficient to define the state of compaction.

Further study by VandenBerg (1966) indicated that the state of compaction in a soil cannot be adequately described with only the mean normal stress. He observed that the maximum shear stress (τ_{max}) applied to soil plays an important role in determining the final state of compaction, and proposed the following functional relationship:

$$\rho = f(\sigma_m + a\ \tau_{max}) \qquad [2]$$

where ρ = bulk density

a = constant representing soil properties

Bailey and VandenBerg (1968) later developed the following specific relationship:

$$\frac{1}{\rho} = B \log\sqrt{(\sigma_m^2 + \tau_{max}^2)} + C \frac{\tau_{max}}{\sigma_m} + D \qquad [3]$$

where B,C,and D are experimentally determined soil parameters

3.4 FINITE ELEMENT ANALYSIS OF SOIL-MACHINE INTERACTION

The past twenty years have witnessed rapid increase in the use of the finite element procedure for solving boundary value problems in many disciplines. During the 1960's many employed this procedure for solving complex boundary value problems in the field of soil mechanics (Clough and Woodward, 1967; Girijavallabhan and Reece, 1968). More recently the finite element method has been used to evaluate various aspects of the machine-soil interaction problem. Some particular advantages of the finite element procedure are:

1. A body of soil composed of any number of soil types may be evaluated.
2. Displacement and stress boundary conditions at any point in the soil may be modeled.

3. Many types and combinations of loads may be applied to the soil.
4. The nonlinear stress-strain behavior of soil may be incorporated into the analysis by using incremental loading techniques.
5. Any degree of accuracy may be attained by simply increasing the number of elements and/or loading increments.

Perumpral (1969) was the first to analyze the problem of soil-machine interaction using the finite element method. The soil response due to loading by a rubber-tired tractor was analyzed for both the static and dynamic loading conditions.

In modeling the soil response beneath a stationary tractor tire, Perumpral approximated the elliptical tire footprint with a circle of equivalent area. The problem was idealized as an axisymmetric problem with the tractor load uniformly distributed over the contact area. Quadrilateral elements with eight degrees of freedom were used to idealize the system. Due to symmetry, only one half of the system was analyzed. The nonlinear behavior of soil was incorporated into the analysis with the help of an iterative technique. An octahedral stress-strain relationship developed from triaxial test results was used for the

nonlinear analysis. Perumpral's predicted stress distribution beneath a stationary tractor tire agreed well with the stress distribution obtained from the Boussinesq equations. However, his predictions were slightly higher than experimentally observed stresses.

A plane strain analysis was conducted for the moving wheel problem. For better approximation of the curved soil-wheel interface, triangular elements were employed for idealization. Boundary loads considered during the analysis included the radial and tangential stresses measured at the interface of a moving rigid wheel by Onafeko and Reece (1967). Since the stress-strain relationship for the soil was not available, the potential use of the procedure for solving soil-wheel interaction problems was demonstrated by assuming a linear elastic soil response. Results of this analysis showed stress bulbs and how they are shifted depending on wheel slip (Perumpral, et al., 1971).

Yong and Fattah (1976) also used the finite element method to predict the stresses and deformations in soil beneath a moving rigid wheel. Nonlinear analysis of the plane strain problem was conducted using an incremental loading procedure followed by unloading to simulate the dynamic response of soil resulting from the passage of a wheel. This method enabled them to predict soil rebound due

to unloading. An octahedral stress-strain relationship was developed from triaxial compression tests. Displacement boundary conditions rather than load boundary conditions were used for the analysis. A geometrical analysis of the moving wheel gave the following equations for calculating the X and Y coordinates of displacements at the wheel-soil interface:

$$X = r_i (\theta_i - \theta) - r (\sin \theta_i - \sin \theta) \quad [4]$$

$$Y = r (\cos \theta - \cos \theta_i) \quad [5]$$

where r = rolling radius of the wheel

r_i = distance from wheel center to instantaneous center of motion

θ_i = angle from bottom dead center to the initial location of the point on the wheel rim

θ = angle from bottom dead center to the new location of the point on the wheel rim

This method of determining displacement boundary conditions displayed poor correlation with actual displacements observed using an X-ray photography technique. However, the entire procedure demonstrated the usefulness of the finite element method for predicting soil behavior beneath a moving wheel.

Yong, Fattah, and Boonsinsuk (1978) used the finite element procedure to model the interaction between soil and a flexible tire. They noted that both the tire deformation and soil properties influence the shape of the tire-soil contact area, distribution of load over that area, and wheel slip at the interface. These effects were taken into account by considering energy losses due to deformation and distortion at the tire-soil interface. Boundary conditions were specified as a parabolic load distribution acting over a rectangular contact area. The dimensions of the contact area were calculated on the basis of applied load, tangential stresses, soil characteristics, and elastic tire behavior using a modified Poritsky formula as shown below:

$$\frac{1}{R_1} + \frac{1}{R_2} = \frac{\left(\frac{4P}{a^2\pi}\right)\left[\frac{1 - \nu_2^2}{E_1} + \frac{1 - \nu_1^2}{E_2}\right]}{1 + \frac{K_2^2}{K_1^2}} \qquad [6]$$

where R_1 = undeformed radius of the tire

R_2 = undeformed radius of the soil (∞)

P = tire load

$2a$ = length of contact surface

E_1, E_2 = modulus of elasticity (tire, soil)

ν_1, ν_2 = Poisson's ratio (tire, soil)

K_1, K_2 = constants based on E and ν for each material

The resulting predictions of energy loss displayed excellent correlation with experimentally determined energy losses from drawbar tests.

Yong and Hanna (1977) used the finite element method for analyzing the action of a cutting blade moving through soil. All prior work concerning machine-soil interaction had assumed a continuum of discrete elements joined at the nodes, thus preventing analysis of soil failure and geometrical discontinuities. In order to model soil behavior along shear failure planes they used a special two-dimensional, four-node element. This element was in the form of a line doubled back on itself which could simulate the sliding and separation of adjacent soil particles. The elements were incorporated into the model at the blade-soil interface and along previously determined shear failure planes within the soil mass. Displacement boundary conditions were applied for the analysis and the nonlinear soil response was approximated with an incremental procedure. The octahedral stress-strain relationship was determined from triaxial test results. Yong and Hanna conducted a plane-strain analysis to model the blade-soil interaction. Although this analysis is appropriate for wide

cutting blades,it could lead to inaccurate predictions for narrow cutting blades. The draft force versus tool displacement curve obtained from the finite element analysis agreed well with that obtained from experimental results.

Turner (1982) used the finite element procedure for soil-track interaction studies. A variety of two-dimensional, two-node beam elements represented the vehicle track and suspension system, and a series of nonlinear springs represented the soil. The nonlinear behavior of the soil elements was approximated with the following equation:

$$F = A\ (c + \sigma \tan \phi)\left[1 + \left(\frac{k}{x_2 - x_1}\right)\left(e^{\left(\frac{ix_2}{k}\right)} - e^{\left(\frac{ix_1}{k}\right)}\right)\right] \quad [7]$$

where F = shear force across an element

A = loaded area of an element

c = soil cohesion

ϕ = soil angle of internal friction

σ = applied normal stress

i = slip rate

k = shear deformation modulus of soil

x = distance from forward edge of track to the node under consideration

The Newton-Raphson method was employed for solving nonlinear equations using a series of linear steps. This analysis demonstrated reasonable accuracy in predicting the slip-thrust response of soil beneath a tracked vehicle. However, the initial assumption of continuity and the method of modeling the soil preclude an analysis of soil response below the surface, and fail to consider the occurrence of soil flow and soil fracture.

Chapter IV

THE FINITE ELEMENT METHOD

Comprehensive discussions of the finite element method are available in a number of textbooks (Desai, 1979; Desai and Abel, 1972; Zienkiewicz, 1971). Hence, a brief discussion of the steps involved in the finite element formulation for an axisymmetric problem is included in this section.

4.1 DISCRETIZATION

The first step of the finite element method involves the subdivision of a body of material into discrete units called finite elements, which are interconnected at nodal points. A typical two-dimensional, four-node quadrilateral element is shown in Figure 1 with respect to a local coordinate system (s,t) and a global coordinate system (r,z). The displacements (u_i,v_i) at each nodal point are the primary unknowns of the problem.

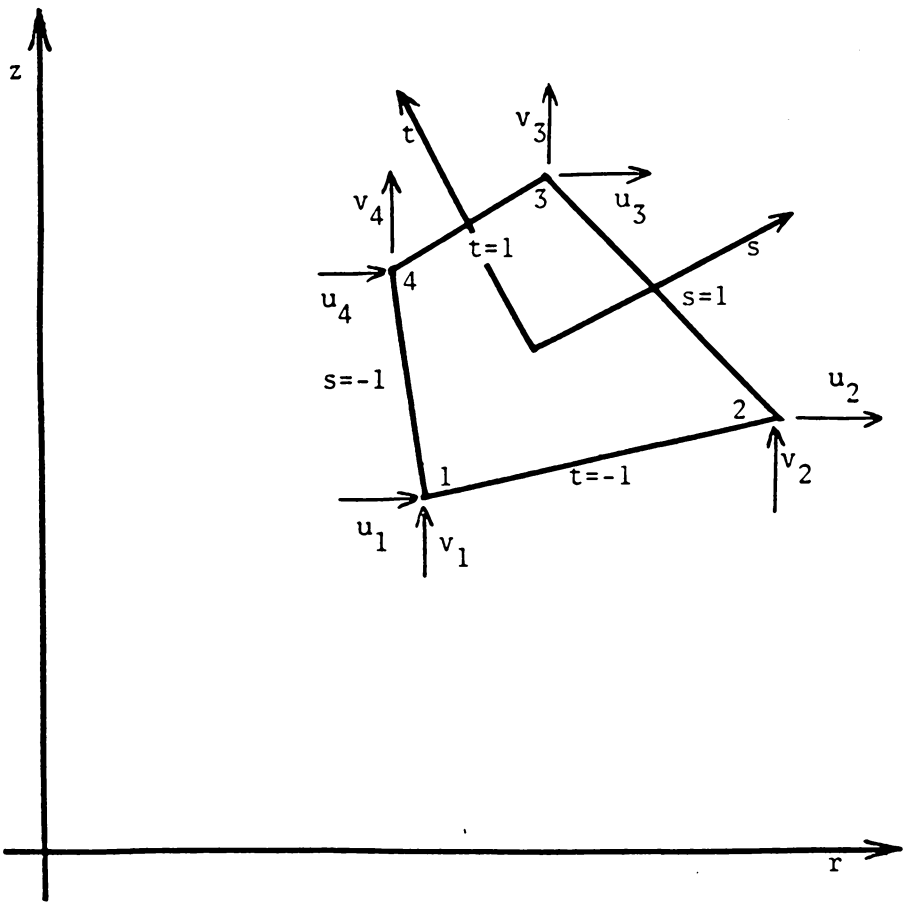

Figure 1: Generalized two-dimensional, four-node quadrilateral finite element.

4.2 APPROXIMATION FUNCTIONS

The displacements at any point within an element are expressed in terms of the nodal displacements through a set of assumed approximation functions of the following form:

$$\{u\} = [N]\ \{q\} \qquad [8]$$

where $\{u\}$ = displacement vector

$[N]$ = matrix of approximation functions

$\{q\}$ = nodal displacement vector

The approximation functions may be of any order, depending upon the type of element chosen for the analysis. For the two-dimensional, four-node quadrilateral element the approximation functions are described by the following equation:

$$N_i = 0.25\ (1 + ss_i)\ (1 + tt_i) \qquad [9]$$

where $i = 1,2,3,4$

N_i = approximation function at node i

s,t = local coordinates

s_i, t_i = local coordinates of node i

4.3 ELEMENT EQUATIONS

A number of methods may be used to derive the element equations (Desai, 1979; Zienkiewicz, 1971). One method involves taking the variation of the total potential energy and setting it equal to zero. This leads to the following expression of the element stiffness equation:

$$[k]\ \{q\} = \{Q\} \qquad [10]$$

where $[k] = \int_{VOL} [B]^T\ [C]\ [B]\ dV$

= element stiffness matrix

[B] = strain-displacement transformation matrix obtained from the derivative of the [N] matrix

[C] = constitutive matrix; describes the stress-strain relationship of the material

{Q} = element load vector

4.4 ASSEMBLAGE

The entire set of stiffness equations for the individual elements are assembled by the direct stiffness method to obtain the following global stiffness equation:

$$[\overline{K}]\ \{\overline{q}\} = \{\overline{Q}\} \qquad [11]$$

where $[\overline{K}]$ = global stiffness matrix

$\{\overline{q}\}$ = global nodal displacement vector

$\{\overline{Q}\}$ = global load vector

4.5 SOLUTION FOR PRIMARY UNKNOWNS

After introducing the appropriate boundary conditions, the global stiffness equation is solved for the primary unknowns using the frontal solution technique. This technique assembles and eliminates variables simultaneously at the element level, thus saving computer memory space.

4.6 SOLUTION FOR SECONDARY UNKNOWNS

Strains and stresses at the centroid of each element are computed using the following two equations:

$$\{\varepsilon\} = [B]\ \{q\} \qquad [12]$$

$$\{\sigma\} = [C]\ \{\varepsilon\} \qquad [13]$$

where $\{\varepsilon\}$ = element strain vector

$\{\sigma\}$ = element stress vector

Chapter V

PROCEDURE

This study involved adopting a finite element program for predicting multipass effects of wheel loadings on soil compaction by taking the nonlinear material characteristics of soil into consideration. Responses of two soil types were studied using this procedure. The wheel-soil interaction problem was analyzed as an axisymmetric problem.

5.1 FINITE ELEMENT PROGRAM MODIFICATION

The finite element computer program[1] used in this study is a modification of a program originally developed for the linear elastic analysis of two-dimensional problems. A number of changes were made within the program for the purposes of this study. These included an incremental procedure for nonlinear analysis, loading and unloading of soils to simulate multiple wheel loading, and computation of volumetric strain as an indicator of degree of compaction at the end of each wheel loading. Details of these changes are described in the following sections.

---

[1] The basic finite element program was provided by Dr. T. Kuppusamy, Professor of Civil Engineering, Virginia Tech.

5.1.1 Material Nonlinearity

The first modification made to the basic finite element program was to include a means for modeling material nonlinearity. Naturally occurring soils display a nonlinear stress-strain response to applied loads. A typical stress-strain relationship for soil during loading and unloading is shown in Figure 2.

A hyperbolic model developed by Duncan and Chang (1970) was incorporated into the finite element program to model nonlinear soil behavior. The hyperbolic model was selected due to its generality. It models the nonlinear behavior of any natural soil using data from triaxial compression tests of the soil at various confining pressures. The equation developed by Duncan and Chang for the hyperbolic model is shown below:

$$E_t = 1 - \left[\frac{R_f \, (1 - \sin \phi)(\sigma_1 - \sigma_3)}{2c \cos \phi + 2(\sigma_3 + p_a)(\sin \phi)} \right]^2 K \, p_a \left[\frac{\sigma_3 + p_a}{p_a} \right]^n \quad [14]$$

where E_t = tangent modulus of elasticity

ϕ = angle of internal friction

c = cohesion

p_a = atmospheric pressure

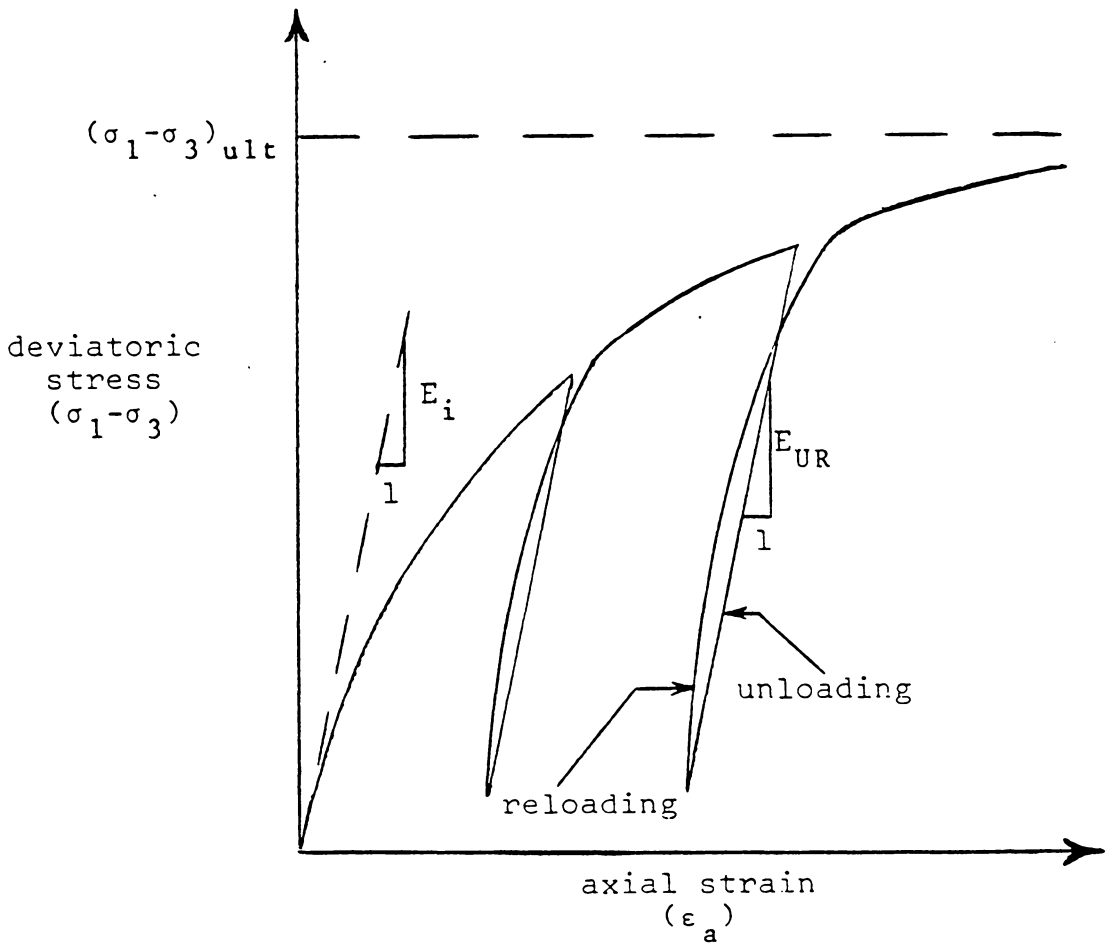

Figure 2: A typical stress-strain relationship for soil during loading and unloading with constant confining pressure (σ_3).

σ_1 = major principal stress

σ_3 = minor principal stress (confining pressure)

R_f = failure ratio; the ratio between the deviatoric stress at failure and the ultimate deviatoric stress

K,n = dimensionless numbers

Equation 14 was used to calculate the modulus of elasticity (E_t) for each element within the soil mass, depending upon the state of stress.

The nonlinear material characteristic shown in Figure 2 was incorporated with an incremental loading technique. For the incremental technique, the total boundary load was applied in a series of small load increments. The finite element analysis was carried out for each incremental load to determine the state of stress and strain at the centroid of each element of soil. At the end of each increment Equation 14 was used to calculate a new modulus of elasticity (E_t) for each element based on the state of stress. Thus, the hyperbolic curve in Figure 2 was approximated by a series of straight lines, representing the load increments. The incremental technique was chosen for this analysis because of its compatibility with the finite element method, and because it is possible to consider

initial stresses in soil due to body weight (Duncan and Chang, 1970).

5.1.2 Unloading and Reloading

Soil response to repeated passes of a pneumatic tire was considered during the study. Duncan and Chang (1970) observed an almost linear elastic response during unloading and reloading in naturally occurring soils under constant confining pressure. This unloading-reloading response is shown graphically in Figure 2. In this study the analysis of unloading and reloading resulting from successive tire passes was carried out assuming a constant modulus of elasticity. The following equation was chosen to describe this linear elastic stress-strain relationship:

$$E_{UR} = (K_{UR})(p_a) \qquad [15]$$

where E_{UR} = unloading-reloading modulus of elasticity

K_{UR} = dimensionless number determined from analysis of triaxial compression test data

5.1.3 Volumetric Strain Computation

In this study the volumetric strain experienced by each element due to wheel loading was considered an indicator of the degree of compaction within the soil mass. Hence the volumetric strain of an element of soil was calculated using the following relationship (Poulos and Davis, 1974):

$$\varepsilon_v = \varepsilon_z + \varepsilon_r + \varepsilon_\theta \qquad [16]$$

where ε_v = volumetric strain

ε_z = vertical strain

ε_r = radial strain

ε_θ = tangential strain

Since the values of vertical strain, radial strain, and tangential strain were determined for each element during the analysis, the volumetric strain for each element can be easily computed after each incremental load application.

5.2 LINEAR ELASTIC ANALYSIS FOR MODEL VERIFICATION

The primary purpose for conducting the linear elastic analysis was to examine the validity of the finite element program used in this study. The stress distribution from a uniformly loaded circular flexible footing (see Figure 3) was determined and compared against the published solution.

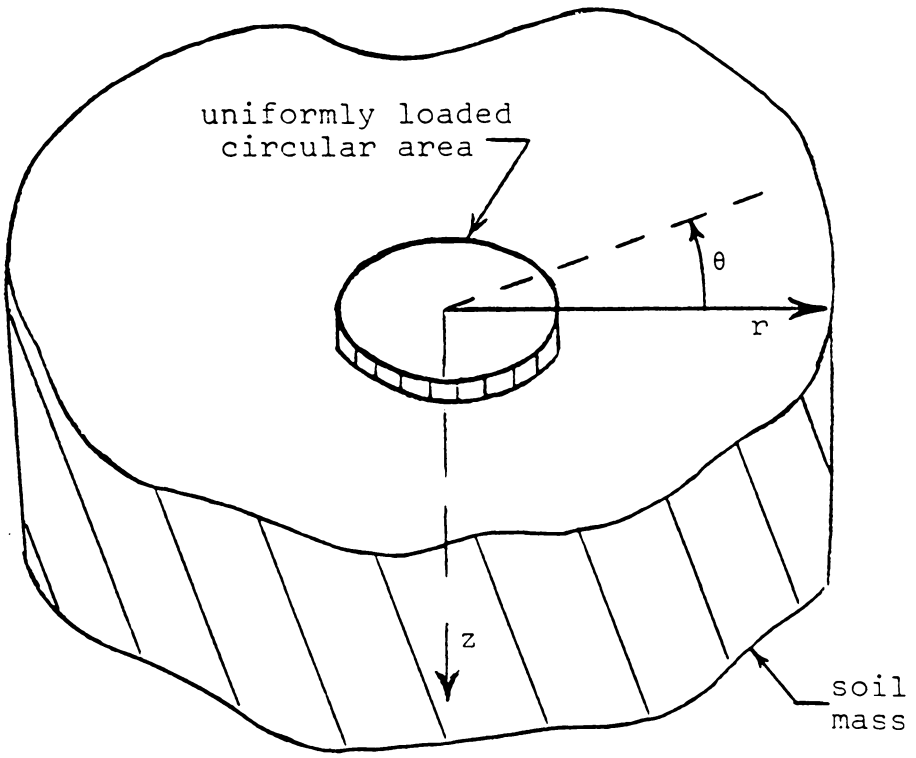

Figure 3: Axisymmetric loading situation with a uniformly distributed load applied over a circular area.

The modulus of elasticity and Poisson's ratio used for the analysis were 27,580 kPa (4000 psi) and 0.42, respectively. A uniform surface pressure of 124 kPa (18 psi) was distributed over a circular area of 50.8 cm (20.0 in.) diameter. Due to symmetry about the vertical (z) axis, only one half of the system was analyzed. The finite element mesh used for this analysis is shown in Figure 4 with a radius (a) of 25.4 cm (10.0 in.). A finer mesh was employed directly beneath the applied load because of the stress concentration in this region. Boundaries of the idealized system in the radial and vertical directions were chosen at a substantial distance from the applied load to minimize boundary influences. Thus, Face 2 and Face 3 in Figure 4 were established at a depth and width, respectively, of six times the radius of the loaded surface area. The nodes on Face 1 and Face 3 were set on rollers permitting only vertical displacement. The nodes on the soil surface and on Face 2 were free to displace in both the radial and vertical directions. To demonstrate the accuracy of this finite element procedure, the finite element predictions of stress were compared graphically with stress distributions obtained from the Boussinesq equations.

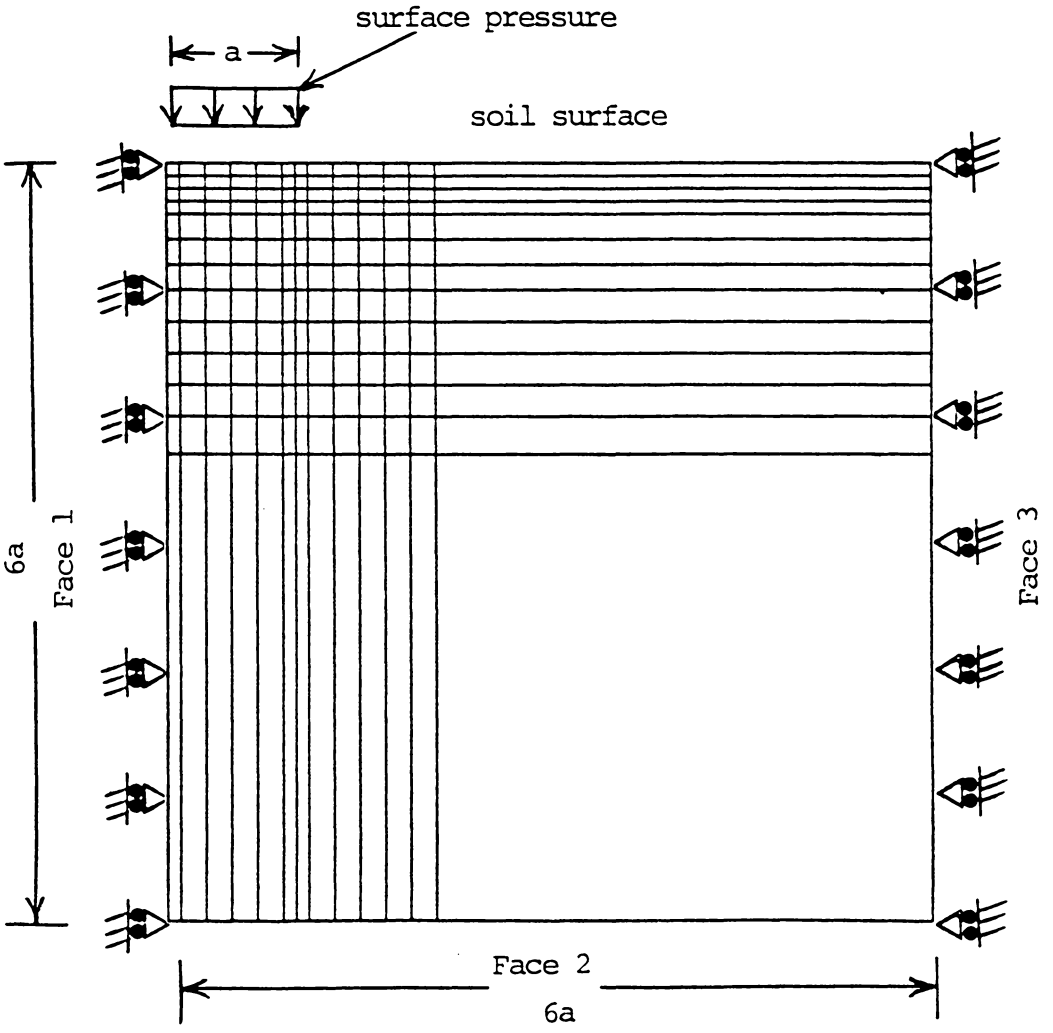

Figure 4: Finite element mesh for linear elastic analysis of stress in soil beneath a 20 inch diameter circular flexible footing.

5.3 ANALYSIS OF SOIL COMPACTION DUE TO MULTIPLE WHEEL LOADING

After verification of the finite element program, nonlinear analyses were conducted to determine soil compaction resulting from multiple wheel loading for the following three tire-soil combinations:

1. Multiple passes of an 18.4-38 bias ply tire in clay.
2. Multiple passes of an 18.4-38 bias ply tire in sand.
3. Multiple passes of a larger tire in clay.

5.3.1 18.4-38 Bias Ply Tire in Clay

In this study the tire-soil interaction problem was modeled as a two-dimensional, axisymmetric problem. This was accomplished by approximating the elliptical tire footprint with a circle of equivalent area, and by assuming that the contact pressure was uniformly distributed over the circular contact area. Due to symmetry about the vertical (z) axis, stress and strain within the soil mass are constant in the tangential (θ) direction. Thus the state of stress and strain at every point in the soil is determined by analyzing any vertical half-plane which has the radial (r) axis and vertical (z) axis as its boundaries.

Data on the contact area and contact pressure for standard tractor tires was obtained from Deere and Company (Table 1) and used for specifying boundary loads. The

TABLE 1

Pneumatic tractor tires and contact pressures (Deere & Co.)

Tire Type	Tire Load	Contact Pressure	Contact Area
Bias Ply 18.4-38 6 ply	23,360 N (5250 lb)	125 kPa (18.1 psi)	1872 cm^2 (290.1 in^2)
Bias Ply 20.8-38 8 ply	30,350 N (6820 lb)	134 kPa (19.4 psi)	2268 cm^2 (351.5 in^2)
Radial Ply 18.4R38 6 ply	23,360 N (5250 lb)	111 kPa (16.1 psi)	2104 cm^2 (326.1 in^2)
Radial Ply 20.8R38 8 ply	30,350 N (6820 lb)	119 kPa (17.2 psi)	2558 cm^2 (396.5 in^2)

loading by an 18.4-38 bias ply tractor tire was modeled as a 124 kPa (18 psi) uniformly distributed surface pressure over a 50.8 cm (20.0 in.) diameter circular area. The finite element mesh developed for this analysis is shown in Figure 5 with a radius (a) of 25.4 cm (10.0 in.). The boundaries of Face 1, Face 2, and Face 3 were all idealized as rollers, permitting nodal displacement in only one direction. Nodal points at the soil surface were free to displace in both the radial and vertical directions.

A clay soil was chosen for this analysis since values of soil parameters describing an agricultural soil were not available. Since the overall goal of this study was to develop the procedure for the finite element analysis of soil compaction due to multiple wheel loadings, it was decided that soil parameters determined and published by Duncan and Chang (1970) for clay and sand should be used. These soil parameters are listed in Table 2.

The first step of the nonlinear analysis was to determine the initial modulus of elasticity (E_i) based upon in situ stresses for each element within the idealized system. The major and minor principal stresses were determined based upon body force and coefficient of earth pressure at rest using the following relationships:

$$\sigma_1 = \rho z \qquad [17]$$

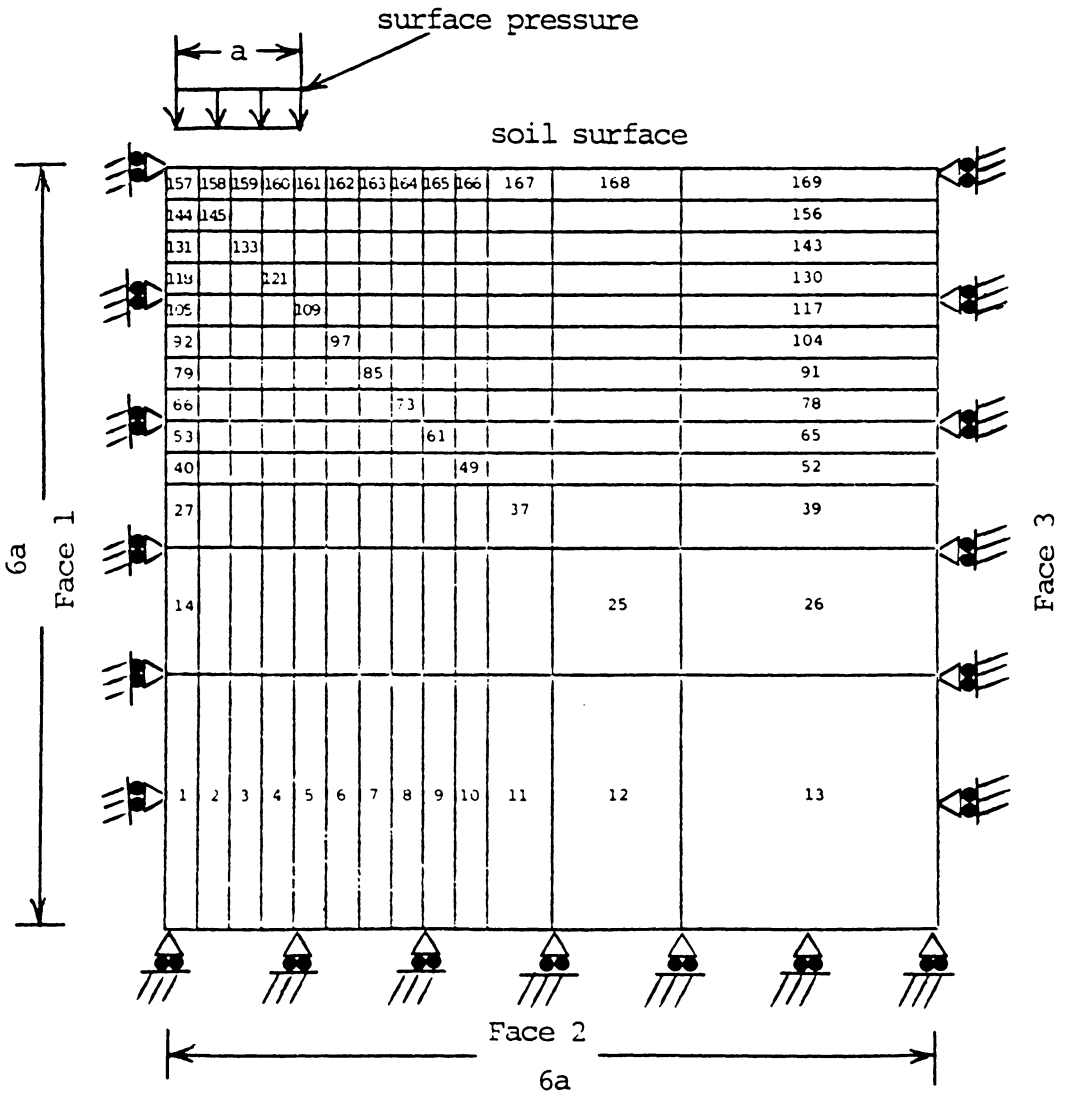

Figure 5: Idealized system for analyzing soil compaction due to multiple wheel loading.

TABLE 2

Soil parameters used for the finite element analysis

	Clay	Sand
Poisson's ratio (ν)	0.48	0.34
soil density (ρ)	1770 kg/m^3 (0.064 lb/in^3)	1467 kg/m^3 (0.053 lb/in^3)
coefficient of earth pressure at rest (K_o)	0.95	0.50
angle of internal friction (ϕ)	0°	30.4°
cohesion (c)	48 kPa (6.9 psi)	0.0 kPa
K	47.0	295.0
K_{UR}	400.0	1090.0
n	0.001	0.65
failure ratio (R_f)	0.90	0.90

$$\sigma_2 = K_o \sigma_1 \qquad [18]$$

where ρ = soil density

z = depth of element centroid below soil surface

K_o = coefficient of earth pressure at rest

The magnitude of K_o varies with soil type. The following equations were used to compute K_o for the two soil types considered during the study (Brooker and Ireland, 1965; Hettiaratchi and Callaghan, 1980):

Clay soil: $$K_o = 0.95 - \sin \phi \qquad [19]$$

Sandy soil: $$K_o = 1.0 - \sin \phi \qquad [20]$$

where ϕ = angle of internal friction

The major and minor principal stress values thus obtained were used in Equation 14 to calculate the initial modulus of elasticity for each element of soil.

The nonlinear analysis of the soil was continued by applying the 124 kPa (18 psi) load in six increments of 20.7 kPa (3 psi) each. After application of each incremental load, the resulting displacements, stresses, and strains within the soil mass were computed. Based on the new state of stress at the end of each load increment, new modulus of

elasticity values were determined for each element and used to analyze the soil response due to the next incremental load. This procedure was continued until the total wheel load had been applied. At this point the soil was unloaded in one step to complete simulation of the first wheel pass. Successive wheel passes were modeled by loading in one step and unloading in one step. The tangent modulus of elasticity for each unloading or reloading step was computed using Equation 15. The increase in soil stiffness due to repeated tire passes was simulated by increasing the magnitude of K_{UR} by 250 after each reloading step. The analysis included five loading-unloading cycles simulating five wheel passes.

Volumetric strain was calculated for each element at the end of each load increment using Equation 16. The values necessary for describing the complete state of stress and strain for an element are listed in Table 3. These values were calculated within the finite element program at the end of each load increment.

5.3.2 18.4-38 Bias Ply Tire in Sand

The simulation of an 18.4-38 bias ply tire in sand was conducted to study the effect of soil properties on the distribution of stress and strain. The idealized system and

TABLE 3

Information available as a result of the finite element analysis

<u>At each node</u>

vertical (z) displacement
radial (r) displacement

<u>At the centroid of each element</u>

radial stress (σ_r)
vertical stress (σ_z)
tangential stress (σ_θ)
shear stress in the rz plane (τ_{rz})
maximum principal stress (σ_1)
minimum principal stress (σ_3)
angle between σ_1 and vertical direction
volumetric strain (ε_v)
tangent Young's modulus of elasticity (E_t)
tangent Poisson's ratio (ν_t)
radial strain (ε_r)
vertical strain (ε_z)
tangential strain (ε_θ)
shear strain in the rz plane (γ_{rz})

boundary conditions applied for this analysis were identical to those used in the preceding analysis. Soil parameters used in this analysis were obtained for a loose silica sand and are listed in Table 2. Five tractor tire passes were modeled, and the K_{UR} value was incremented by 250 for successive unloading-reloading cycles to simulate stiffening of the soil.

5.4 EFFECT OF TIRE SIZE ON SOIL COMPACTION

In order to demonstrate the effect of a wider tire on soil compaction, the same tractor load was distributed over a larger area. The circular area considered for this analysis had a diameter of 61.0 cm (24.0 in.) with a uniform boundary pressure of 86.2 kPa (12.5 psi). This area was selected on an arbitrary basis and it does not represent a specific tire in Table 1. Only the clay soil was considered for this analysis, and the properties listed in Table 2 were used for the simulation. The boundary load of 86.2 kPa (12.5 psi) was applied in five increments of 17.2 kPa (2.5 psi) each. The finite element mesh and corresponding boundary conditions for this analysis are shown in Figure 5 with a radius (a) of 30.5 cm (12.0 in.). The procedure used for the analysis was similar to that described in the previous two sections.

Chapter VI

RESULTS AND DISCUSSION

Results of the finite element analyses are presented and discussed in this chapter. Nondimensional plots of the stress distribution developed from the results of the linear elastic analysis are shown first. This is followed by the results of the three wheel-soil problems considered during the study.

6.1 LINEAR ELASTIC ANALYSIS FOR PROGRAM VERIFICATION

The linear elastic analysis of the flexible footing problem was conducted first to examine the validity of the finite element program. The stress distributions obtained from the analysis are compared against stress distributions obtained theoretically (Harr, 1966). Figure 6 shows the vertical stress (σ_z) observed along selected vertical planes within the soil mass. In general, the finite element predictions agree with the theoretical stress distributions. Some discrepancies between predicted and theoretical stress distribution are noted on the vertical planes where $\frac{r}{a} = 0.8$ and $\frac{r}{a} = 1.2$, near the soil surface. For the vertical plane at $\frac{r}{a} = 0.8$, at shallow depths (where

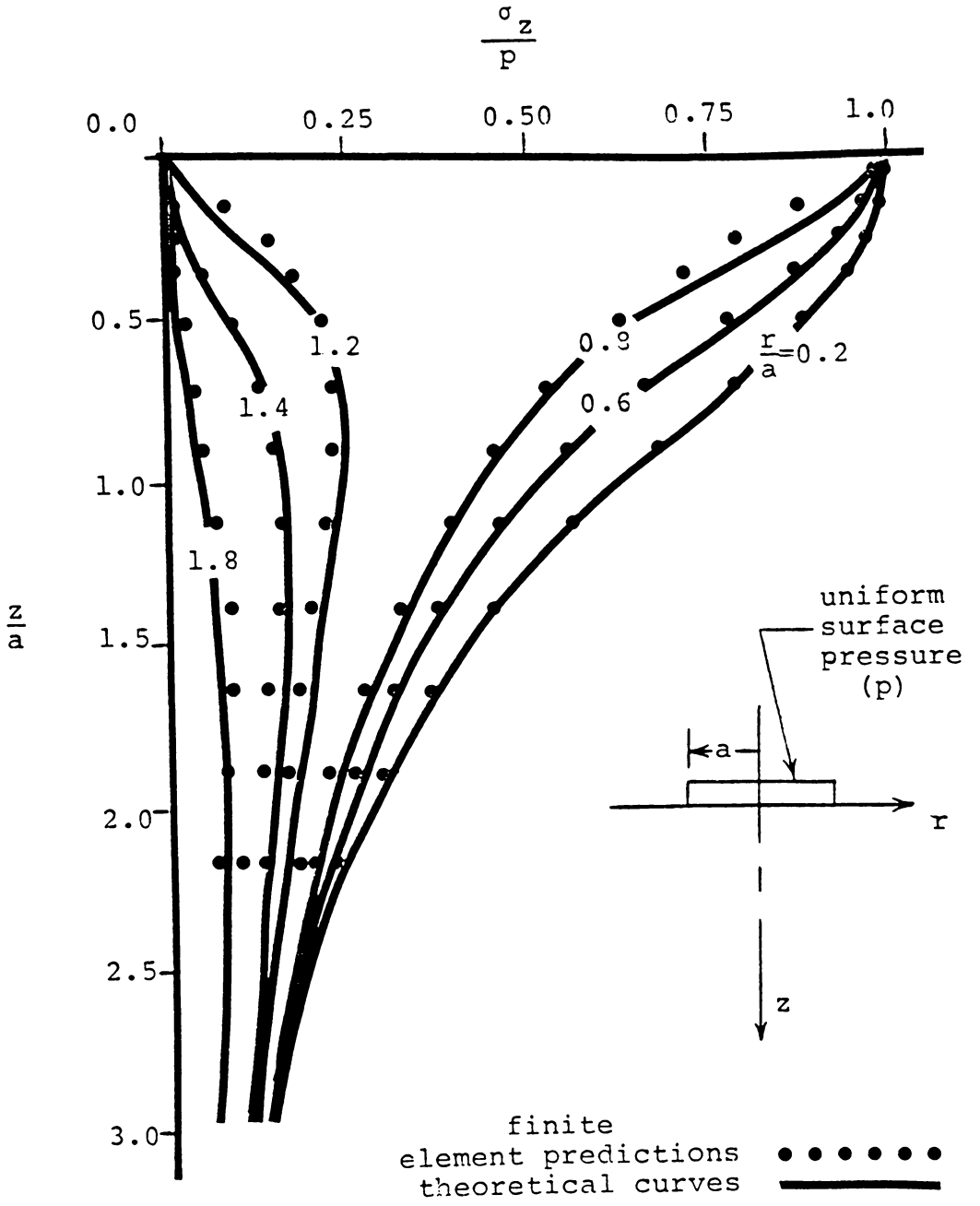

Figure 6: Nondimensional plots of stress distribution on different vertical planes resulting from a uniformly loaded flexible footing.

$\frac{z}{a} < 0.5$), the stress values obtained from the finite element analysis are comparitively lower than those obtained theoretically. On the other hand, on the plane where

$\frac{r}{a} = 1.2$, the finite element predictions are slightly higher. Minor discrepancies of this type should be expected in these regions because of the discontinuity which can occur due to the relative movement of the soil under and outside the loaded area. The finite element program models this discontinuity as a gradual, continuous change in soil displacement. Thus, in this region some discrepancies can be expected. However, in general, the comparison of results from the two different procedures indicates that the finite element model is capable of providing solutions of acceptable accuracy.

6.2 18.4-38 BIAS PLY TIRE IN CLAY

The finite element analysis of multiple loading by an 18.4-38 tire on clay was conducted by considering a 124 kPa (18 psi) load uniformly distributed over a 50.8 cm (20.0 in.) diameter circular area. A vector representation of soil displacement is shown in Figure 7 by plotting the nodal displacements. Since the displacements obtained are very small, they are magnified 3.3 times so that the soil displacement pattern may be more easily observed. Soil

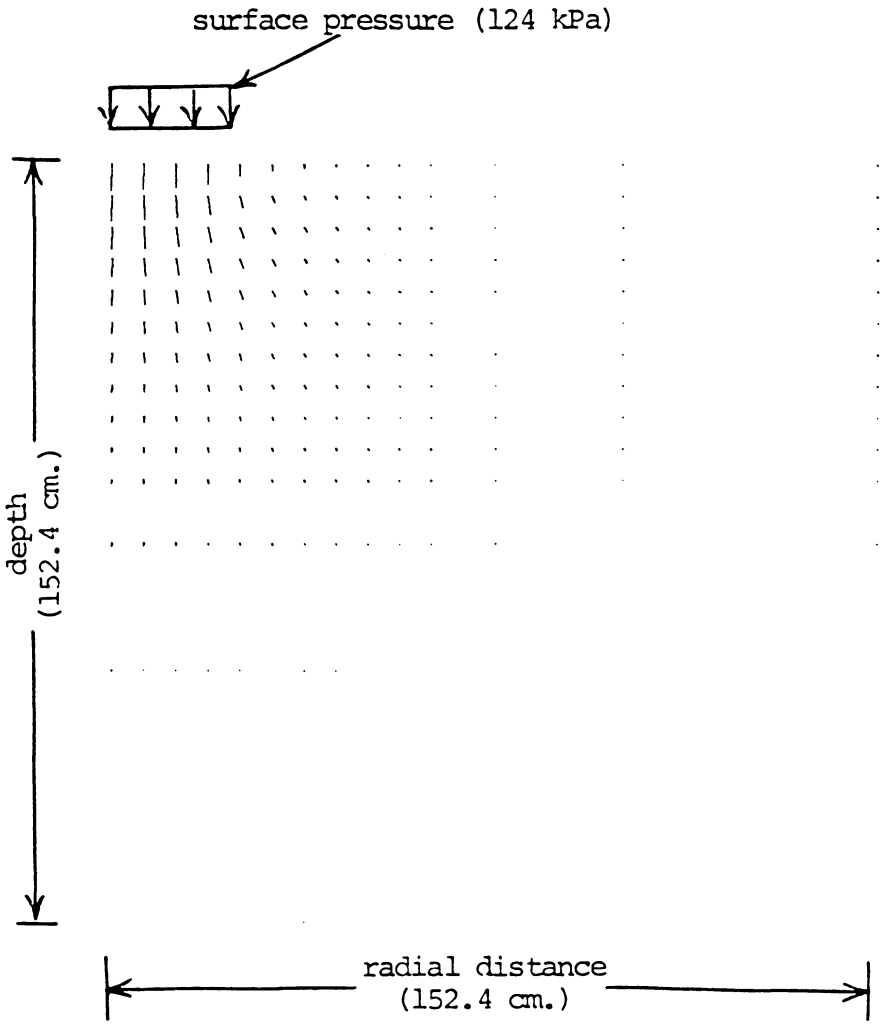

Figure 7: Vector representation of nodal displacements beneath an 18.4-38 bias ply tractor tire in clay.

deformation is found to be negligible at a distance of twice the radius in the radial and vertical directions from the center of the loaded area. As expected, maximum soil displacement occurs directly beneath the center of the surface load. The entire soil mass shows a tendency to displace downward and outward.

Predictions of soil displacement were made for five successive wheel loadings, and the results showed slight increases in displacement with each successive pass. However, the changes in particle orientation were insignificant for repeated loadings and hence are not represented graphically.

Figure 8 shows the vertical stress bulbs due to the wheel loading. As expected, maximum vertical stress occurs directly beneath the center of the surface load, and is approximately equal to the surface load. Simulation of five successive wheel loadings yield vertical stress bulbs identical to the ones shown. This indicates that there is no residual stress build-up in soil due to multiple wheel loadings.

A similar plot of the major principal stress bulbs due to the wheel loading is shown in Figure 9. Maximum principal stress is approximately equal to the surface pressure at the center of the loaded circular area. As

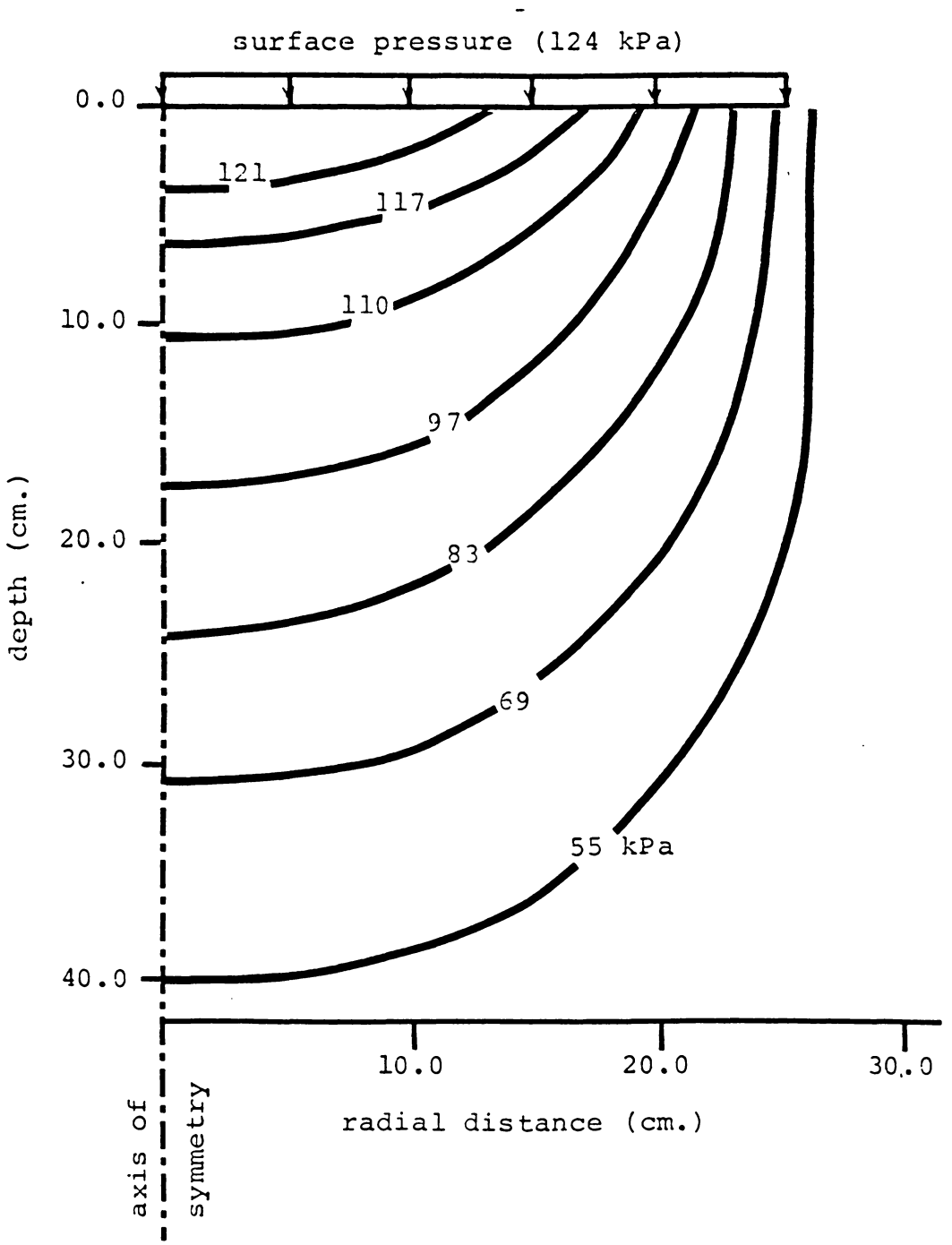

Figure 8: Vertical stress bulbs beneath an 18.4-38 bias ply tractor tire in clay.

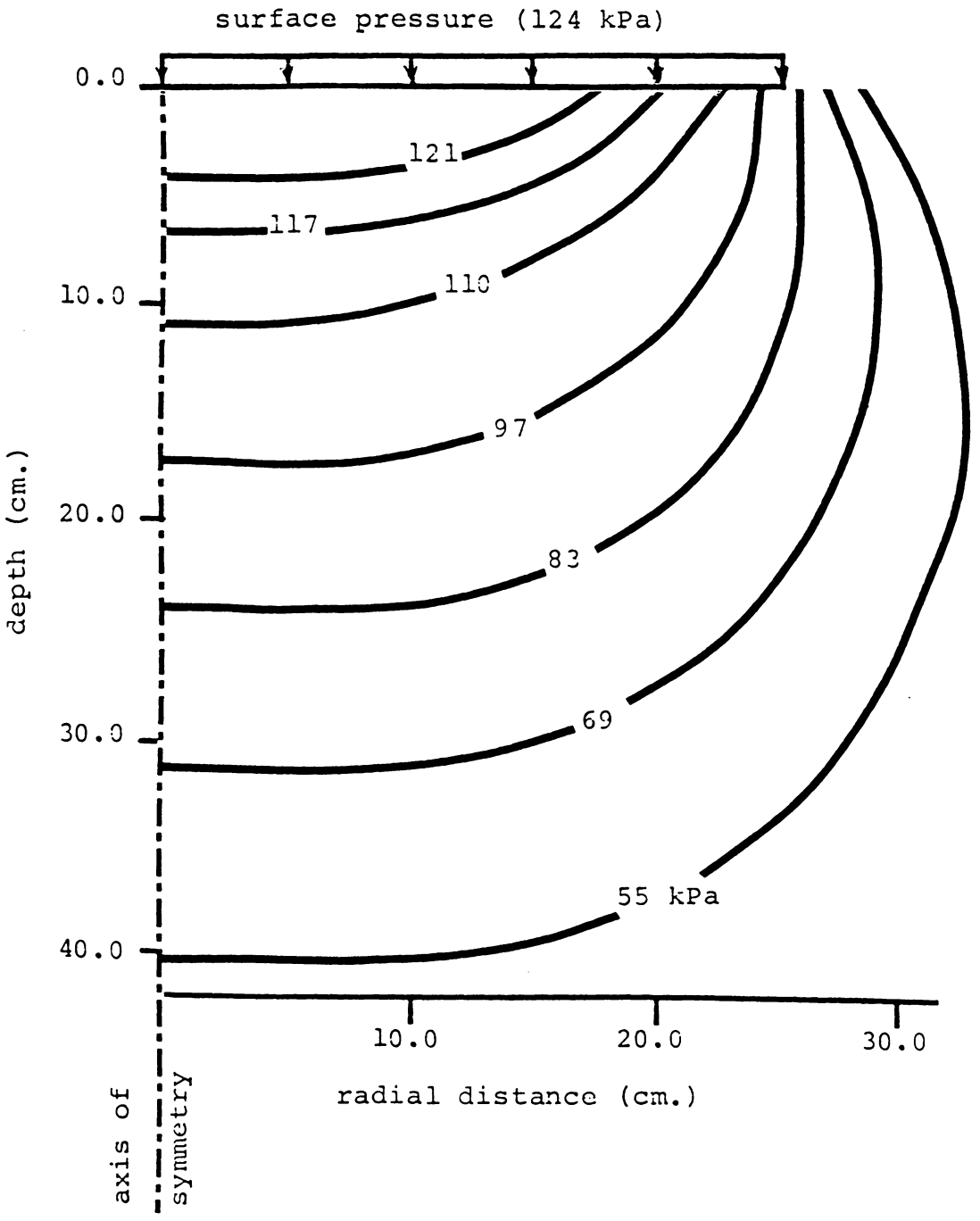

Figure 9: Major principal stress bulbs beneath an 18.4-38 bias ply tractor tire in clay.

expected, along the axis of symmetry $\sigma_1 = \sigma_z$ and $\sigma_3 = \sigma_r$. The major principal stress bulbs are wider than the vertical stress bulbs throughout the soil profile, thus indicating that $\sigma_1 > \sigma_z$ when $r > 0.0$.

Radial stress bulbs obtained from the analysis are shown in Figure 10. Radial stresses are found to be maximum at the soil surface, directly beneath the center of the applied load. At this point $\sigma_r \approx \frac{2}{3} \sigma_z$. However, the magnitudes of radial stress decrease very rapidly with depth, creating a region of high deviatoric stress (σ_1-σ_3) at an approximate depth of 15.2 cm (6.0 in.).

The stress-strain curves for elements 131 and 157 were developed from the results of the finite element analysis by plotting deviatoric stress versus axial strain, and are presented in Figures 11 and 12. These relationships are similar to the hyperbolic stress-strain relationship used for this analysis (see Figure 2) and are considered another indication that the program is operating as it should. In Figures 11 and 12 it can be seen that the curved portion of each graph is composed of six straight-line segments resulting from the incremental loading procedure employed for the nonlinear analysis. As the soil is unloaded the deviatoric stress approaches zero and the soil retains a permanent strain resulting from the wheel loading.

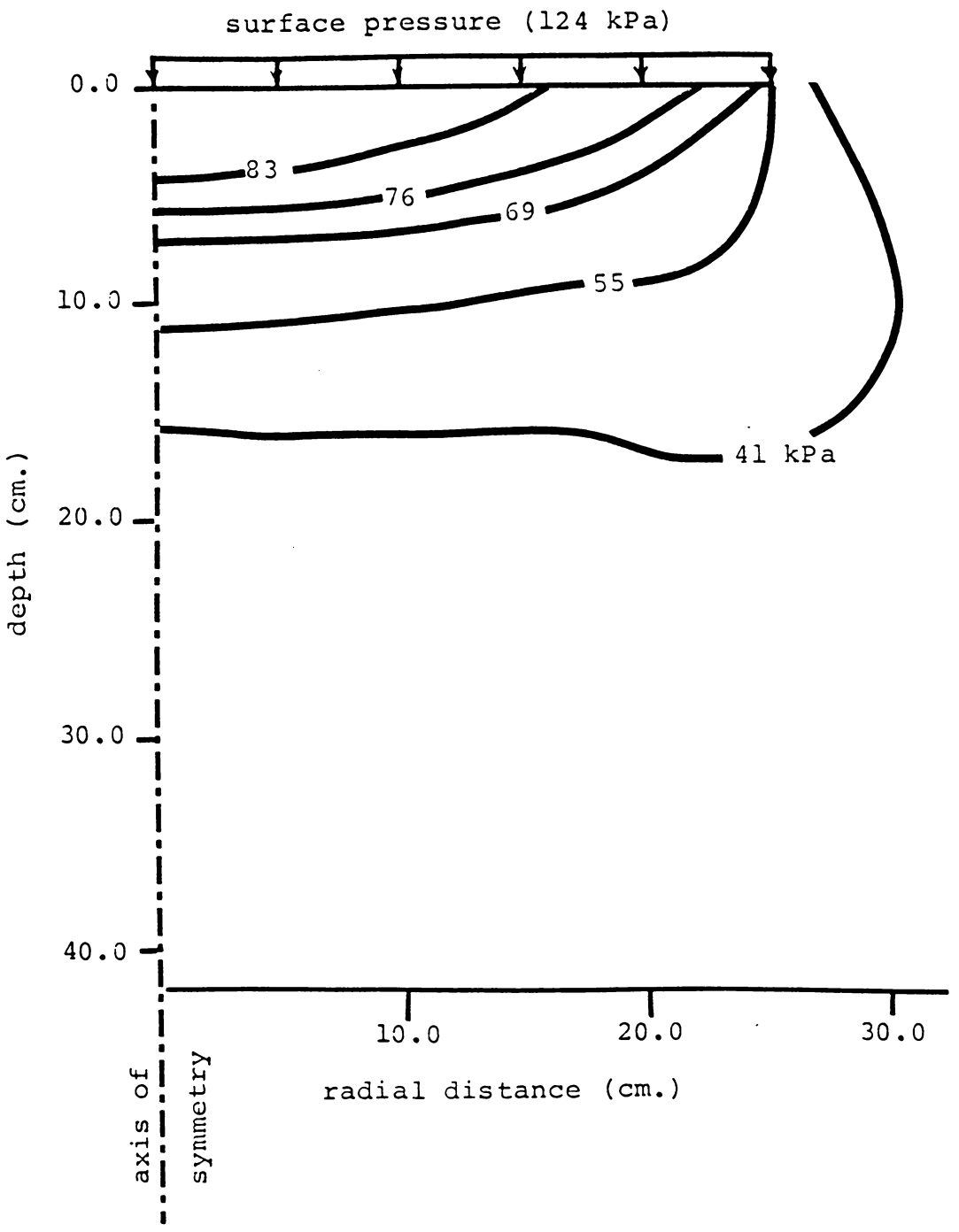

Figure 10: Radial stress bulbs beneath an 18.4-38 bias ply tractor tire in clay.

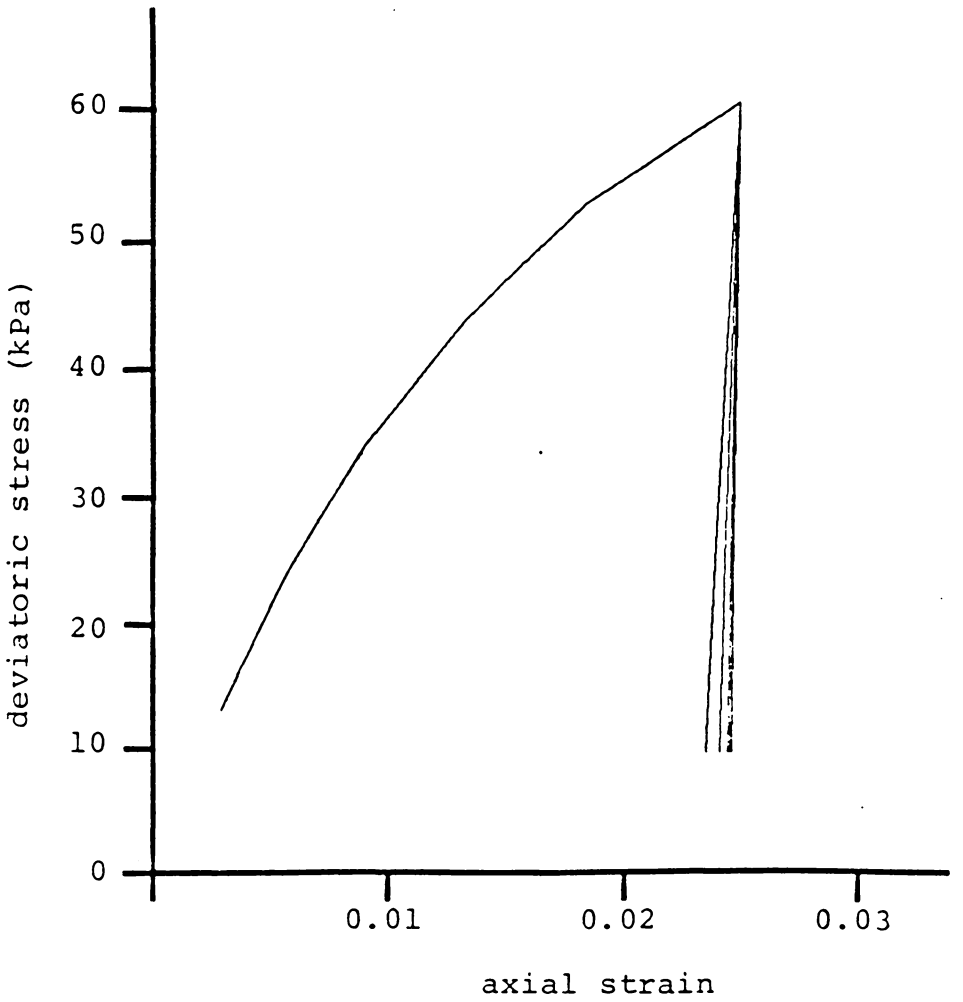

Figure 11: Stress-strain relationship from the results of the finite element analysis for element 131 in clay.

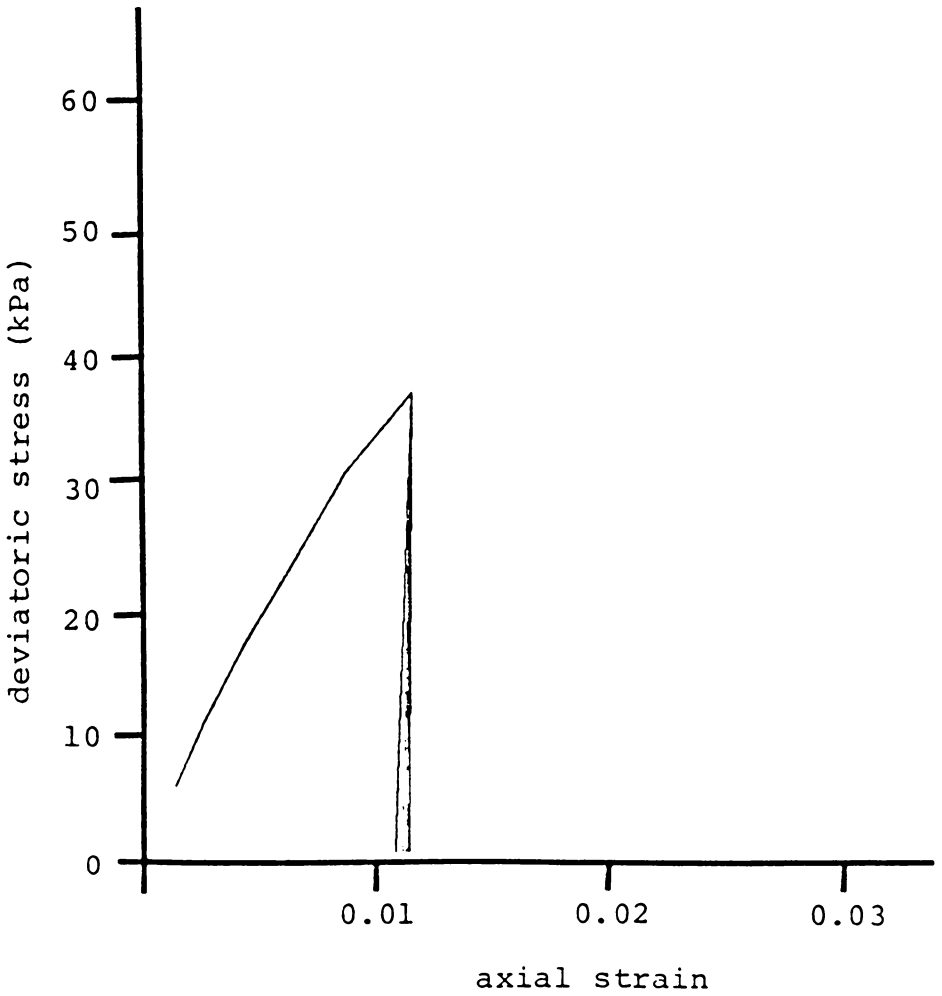

Figure 12: Stress-strain relationship from the results of the finite element analysis for element 157 in clay.

Successive wheel loadings yielded additional residual strain. However, the rate of increase in the residual strain diminished with each successive wheel loading. This trend may indicate that after a certain number of repeated loadings the deformation due to further loading will be elastic.

Element 157, at the soil surface near the center of the loaded area, experiences a maximum deviatoric stress of 35.9 kPa (5.2 psi) and a corresponding axial strain of 0.0113. Element 131 experiences the maximum deviatoric stress of 58.6 kPa (8.5 psi) and a maximum axial strain of 0.0246. The centroid of element 131 is at a depth of 15.9 cm (6.25 in.) below the soil surface.

Contours of residual volumetric strain resulting from five successive wheel loadings are presented in Figures 13 through 17. In all five figures the zone of maximum volumetric strain is at an approximate depth of 10 cm (4 in.), near the axis of symmetry. This indicates that maximum soil compaction due to wheel loading occurs, not at the soil surface, but at a finite depth within the soil profile. A similar observation was made by Chancellor, et al. (1962) during a laboratory study. They found that zones of maximum compaction beneath a loaded piston occurred at a finite depth beneath the soil surface. Porosity contours

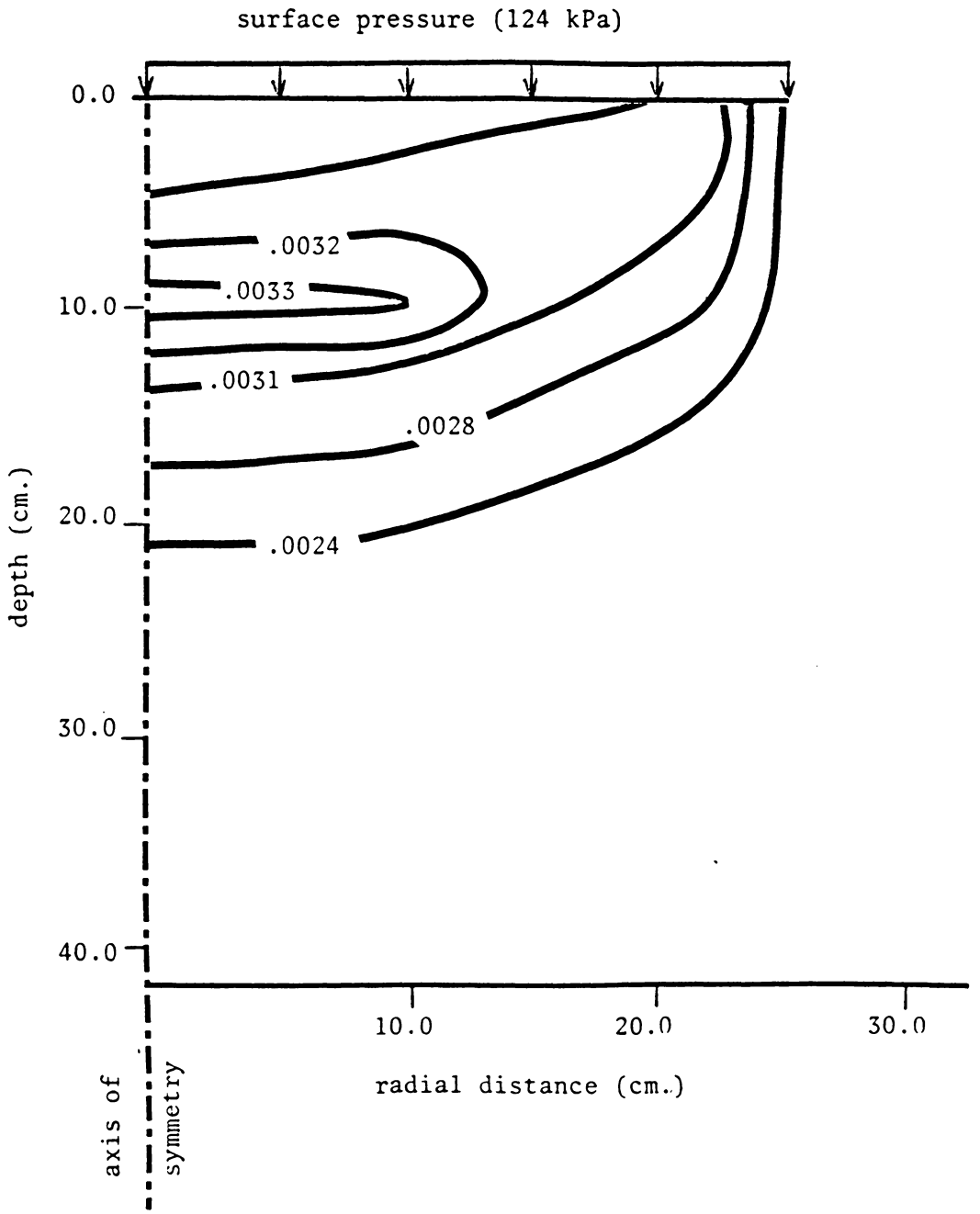

Figure 13: Contours of volumetric strain after one pass of an 18.4-38 bias ply tractor tire in clay.

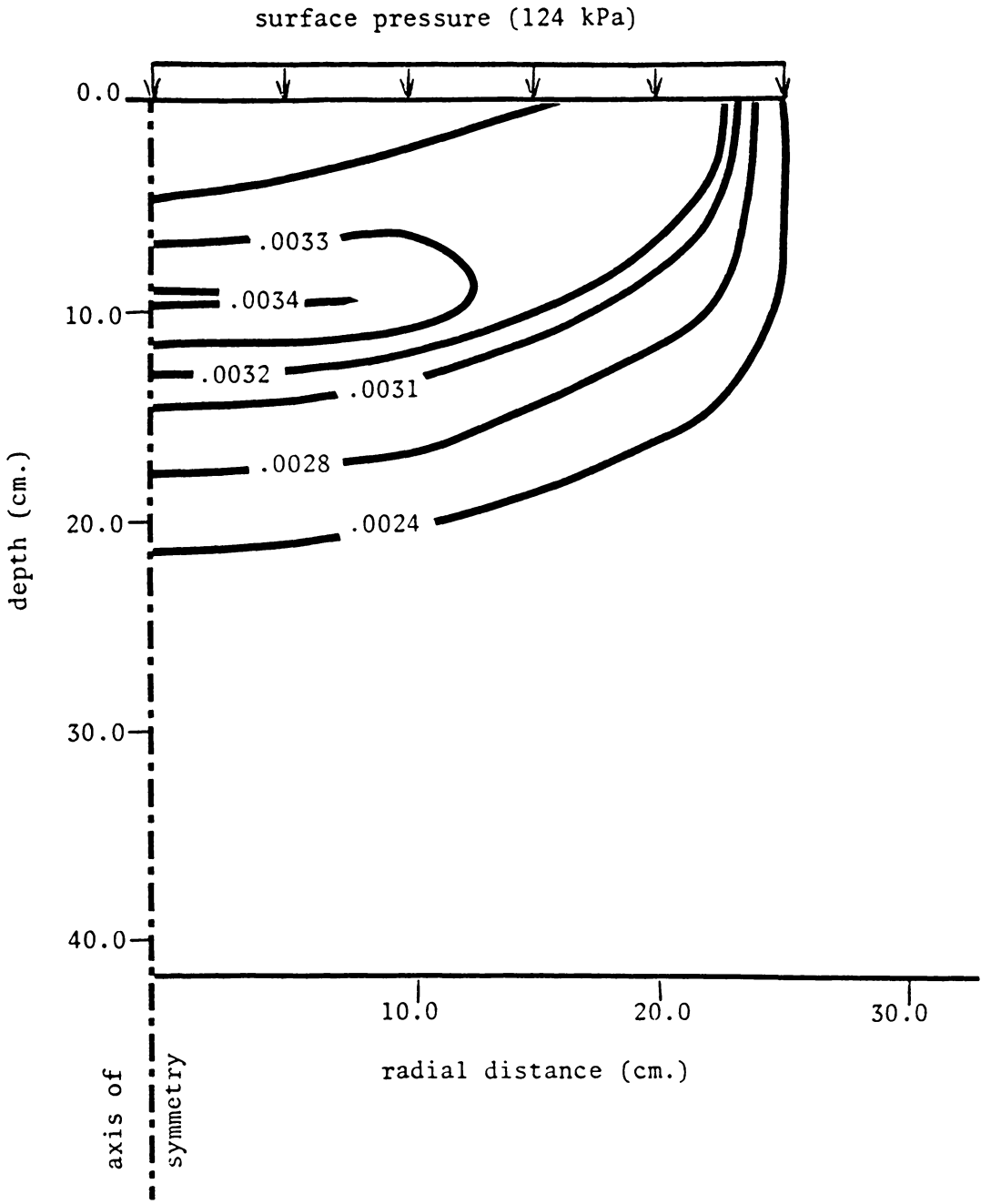

Figure 14: Contours of volumetric strain after two passes of an 18.4-38 bias ply tractor tire in clay.

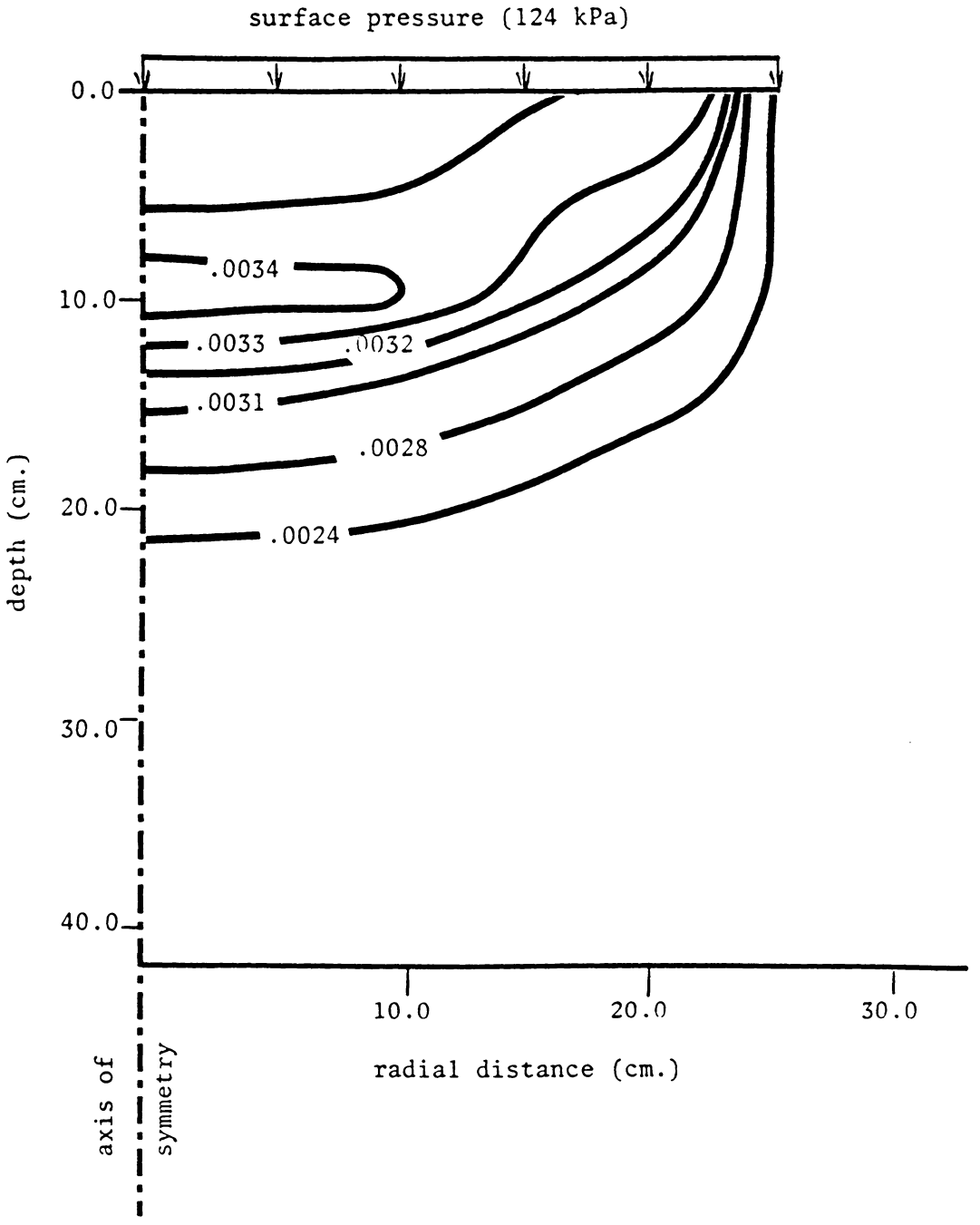

Figure 15: Contours of volumetric strain after three passes of an 18.4-38 bias ply tractor tire in clay.

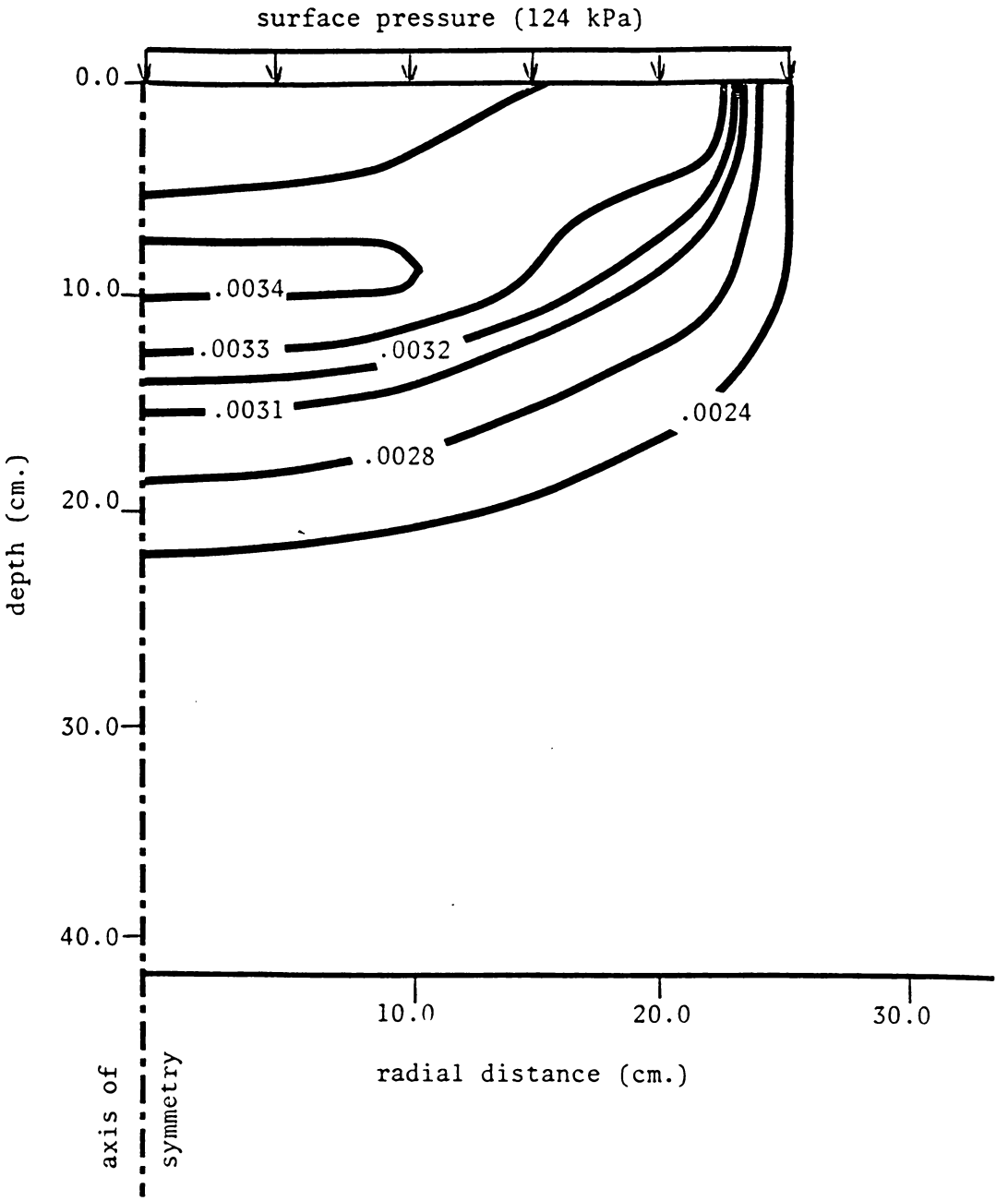

Figure 16: Contours of volumetric strain after four passes of an 18.4-38 bias ply tractor tire in clay.

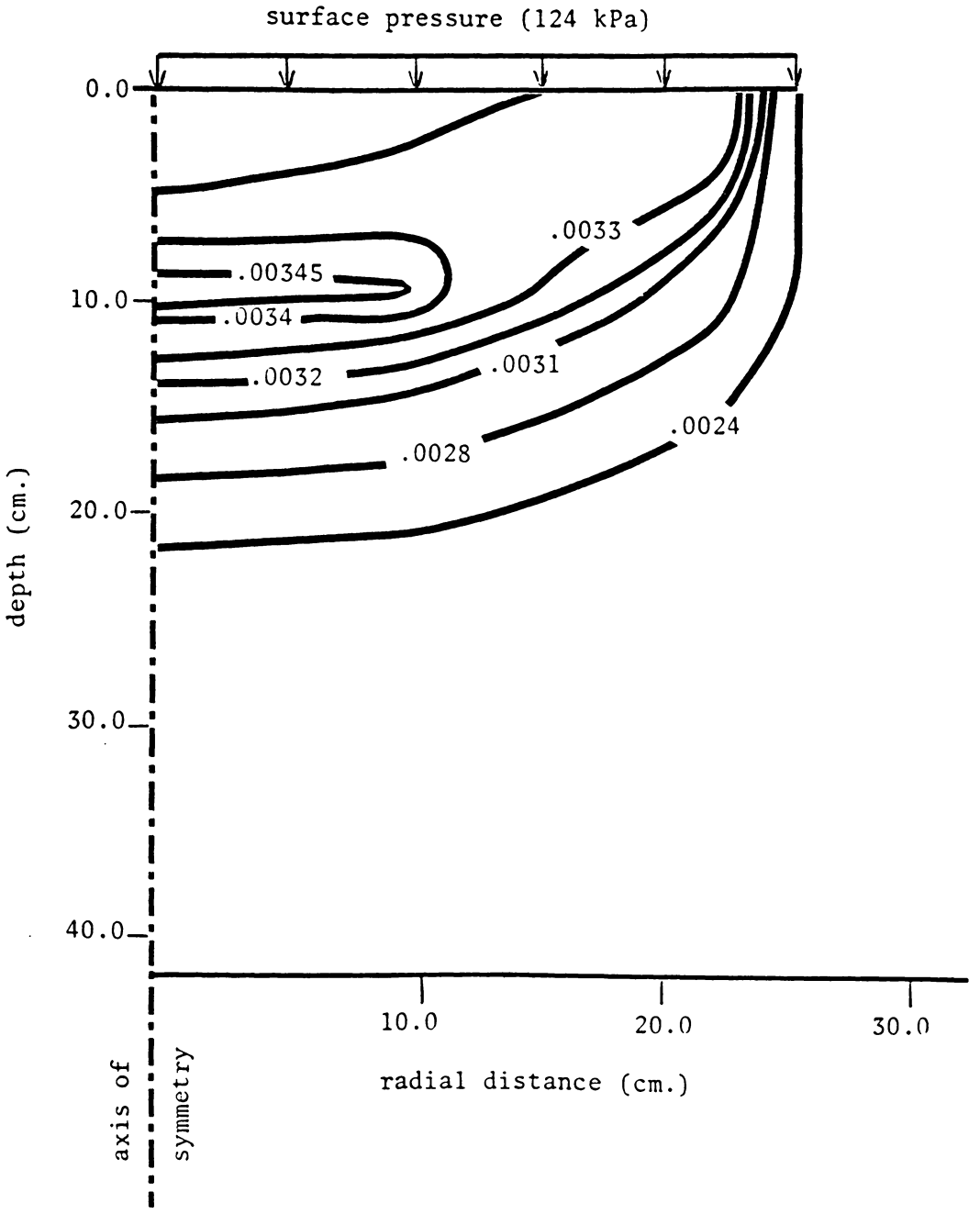

Figure 17: Contours of volumetric strain after five passes of an 18.4-38 bias ply tractor tire in clay.

developed from their study were similar to the volumetric strain contours shown in Figures 13 through 17.

In a recent field study in a Tifton sandy loam soil, Threadgill (1982) noted maximum penetration resistance at soil depths ranging from 15 cm to 30 cm. He attributed this high penetration resistance to the formation of dense soil layers resulting from vehicle traffic. The cone penetrometer profiles are similar in shape to the volumetric strain contours in Figures 13 through 17.

Simulation of each successive wheel loading results in an increase in volumetric strain and the formation of new volumetric strain contours. This is evident in Figures 13 through 17 where the propogation of strain contours is clearly visible. Additional wheel loadings yielded smaller increments of strain due to stiffening of the soil.

The effect of the number of wheel loadings on volumetric strain for element 144 is illustrated in Figure 18. This element experiences the maximum volumetric strain of 0.00348, which corresponds to an increase in soil bulk density from 1770 kg/m^3 to 1776 kg/m^3. 95.7% of the total volumetric strain occurs during the first wheel loading. The second and third wheel loadings yielded increases in volumetric strain of 2.3% and 1.1%, respectively. The shape of the curve in Figure 17 indicated that successive wheel

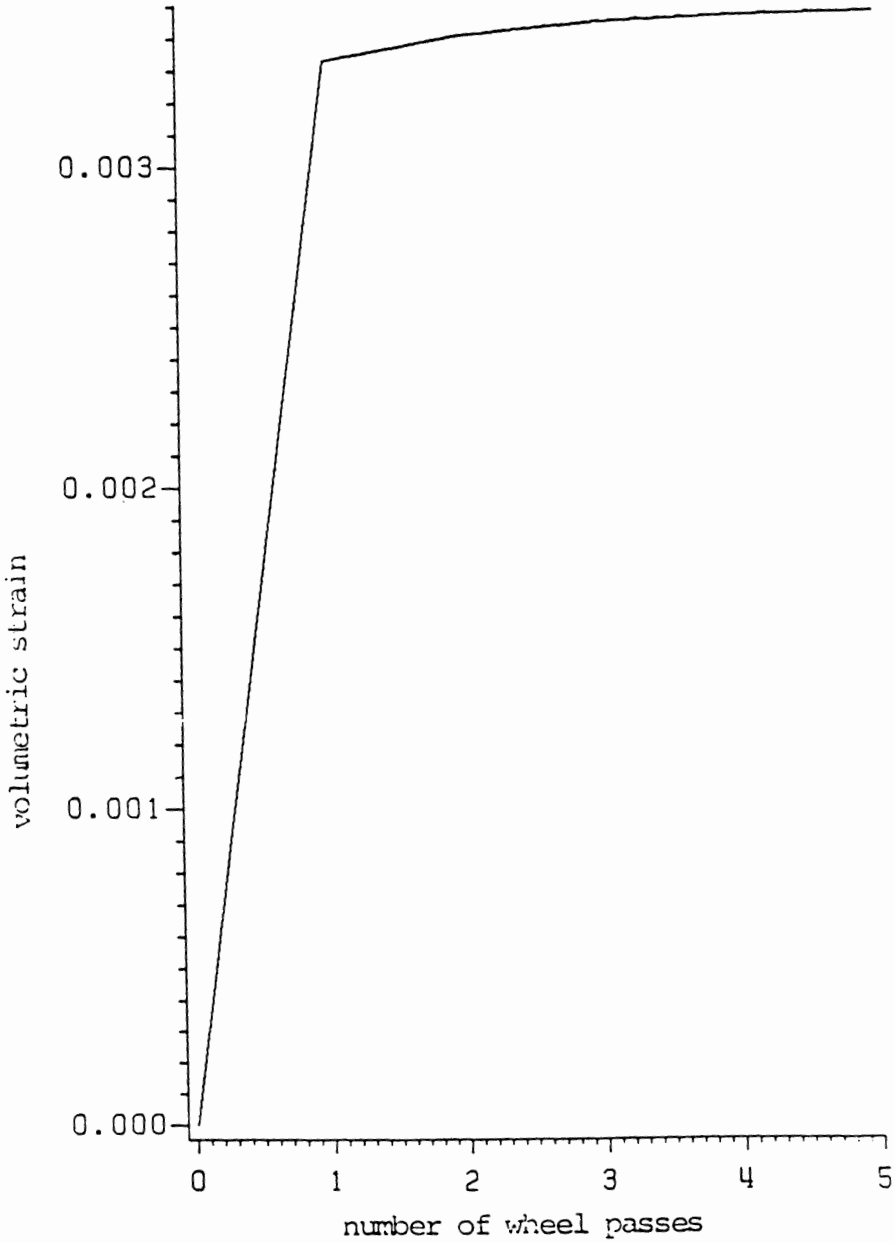

Figure 18: The effect of number of wheel loadings on volumetric strain for element 144 beneath an 18.4-38 bias ply tractor tire in clay.

loadings result in progressively smaller increases in volumetric strain until a final state of maximum compaction is reached for a particular soil.

6.3 18.4-38 BIAS PLY TIRE IN SAND

The finite element analysis was conducted to simulate multiple loading by an 18.4-38 bias ply tire on sand. A vector representation of soil displacement is shown in Figure 19 by plotting the nodal displacements. Displacement vectors are magnified 6.6 times for convenience in observing the overall displacement pattern. The displacement pattern is very similar to that predicted for the clay soil under identical loading conditions (Figure 7). As in clay, the maximum soil displacement occurs directly beneath the center of the loaded area.

Contours of vertical stress, major principal stress, and radial stress obtained from the finite element analysis are shown in Figures 20, 21, and 22, respectively. The stress bulbs are similar to those obtained for the clay soil under identical loading and boundary conditions. However, the magnitudes of vertical stress and major principal stress near the soil surface and adjacent to the axis of symmetry are slightly higher in sand than in clay. This can be explained by noting that the value of the parameter K for

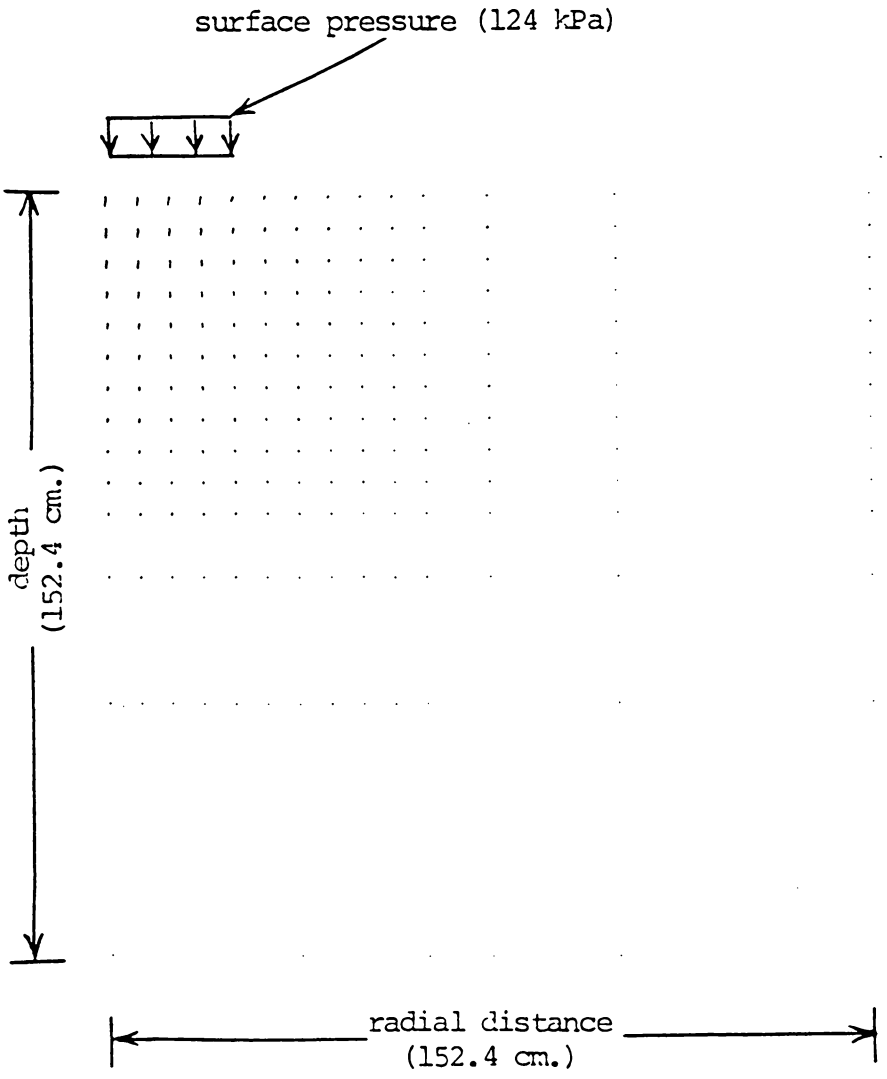

Figure 19: Vector representation of nodal displacements beneath an 18.4-38 bias ply tractor tire in sand.

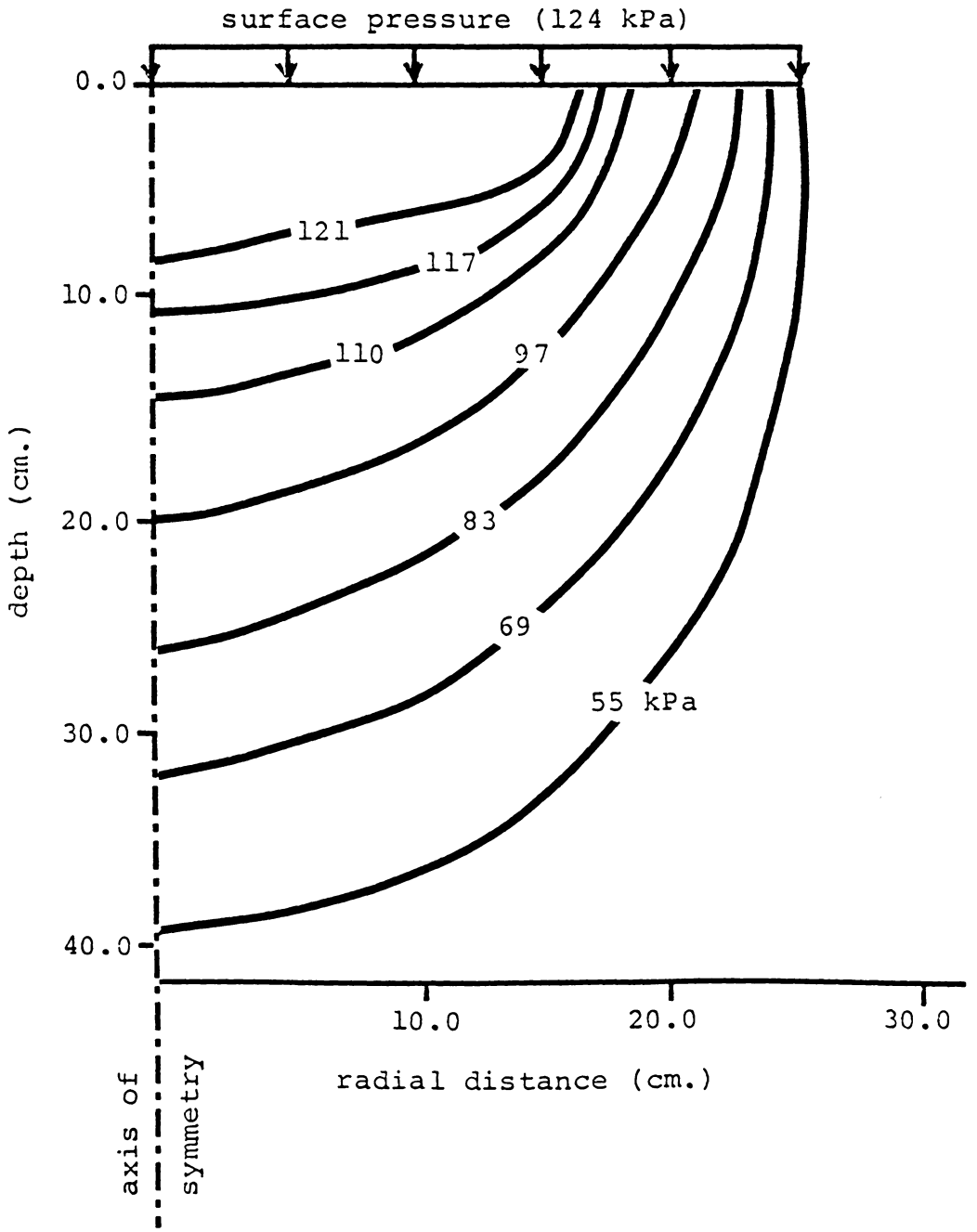

Figure 20: Vertical stress bulbs beneath an 18.4-38 bias ply tractor tire in sand.

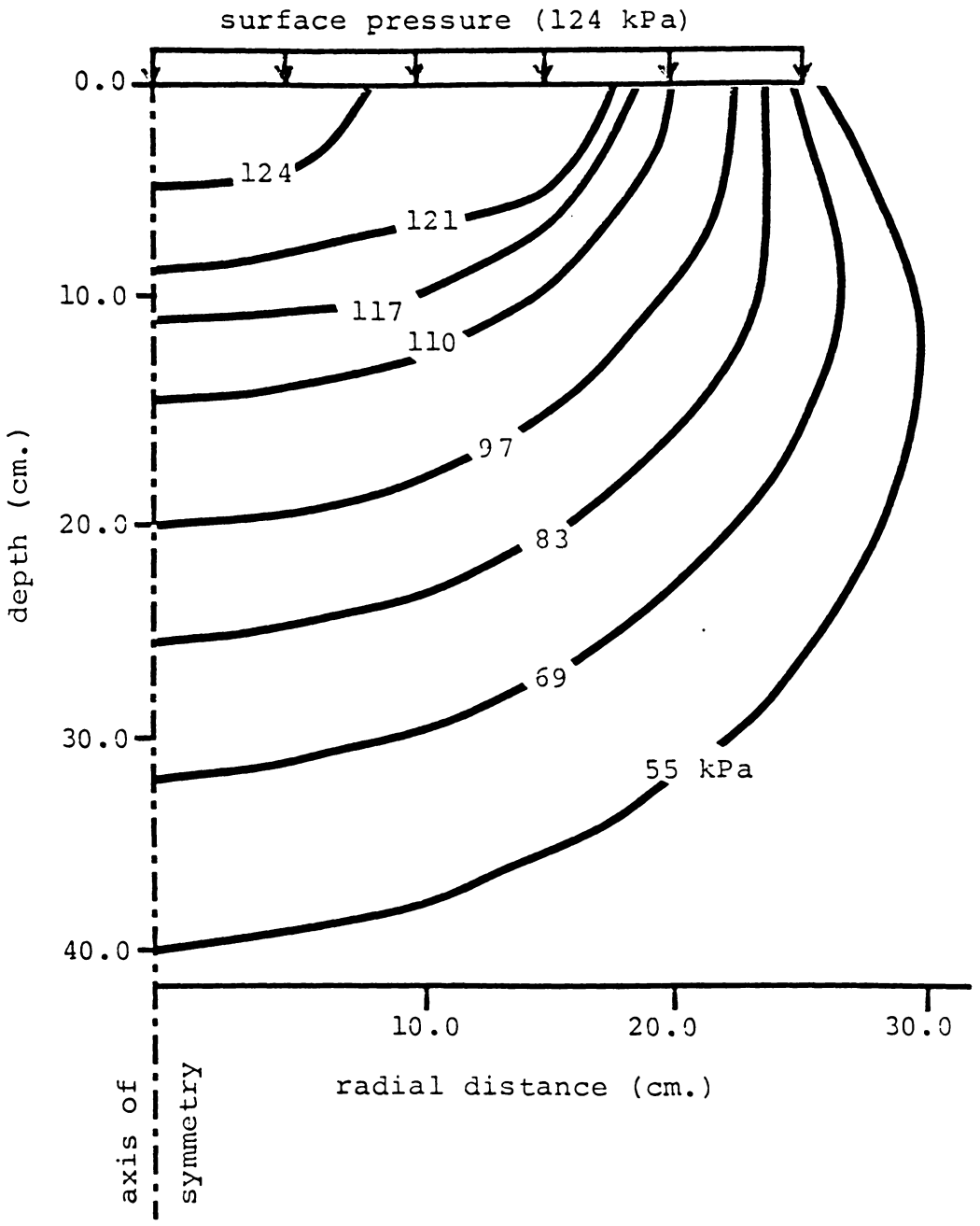

Figure 21: Major principal stress bulbs beneath an 18.4-38 bias ply tractor tire in sand.

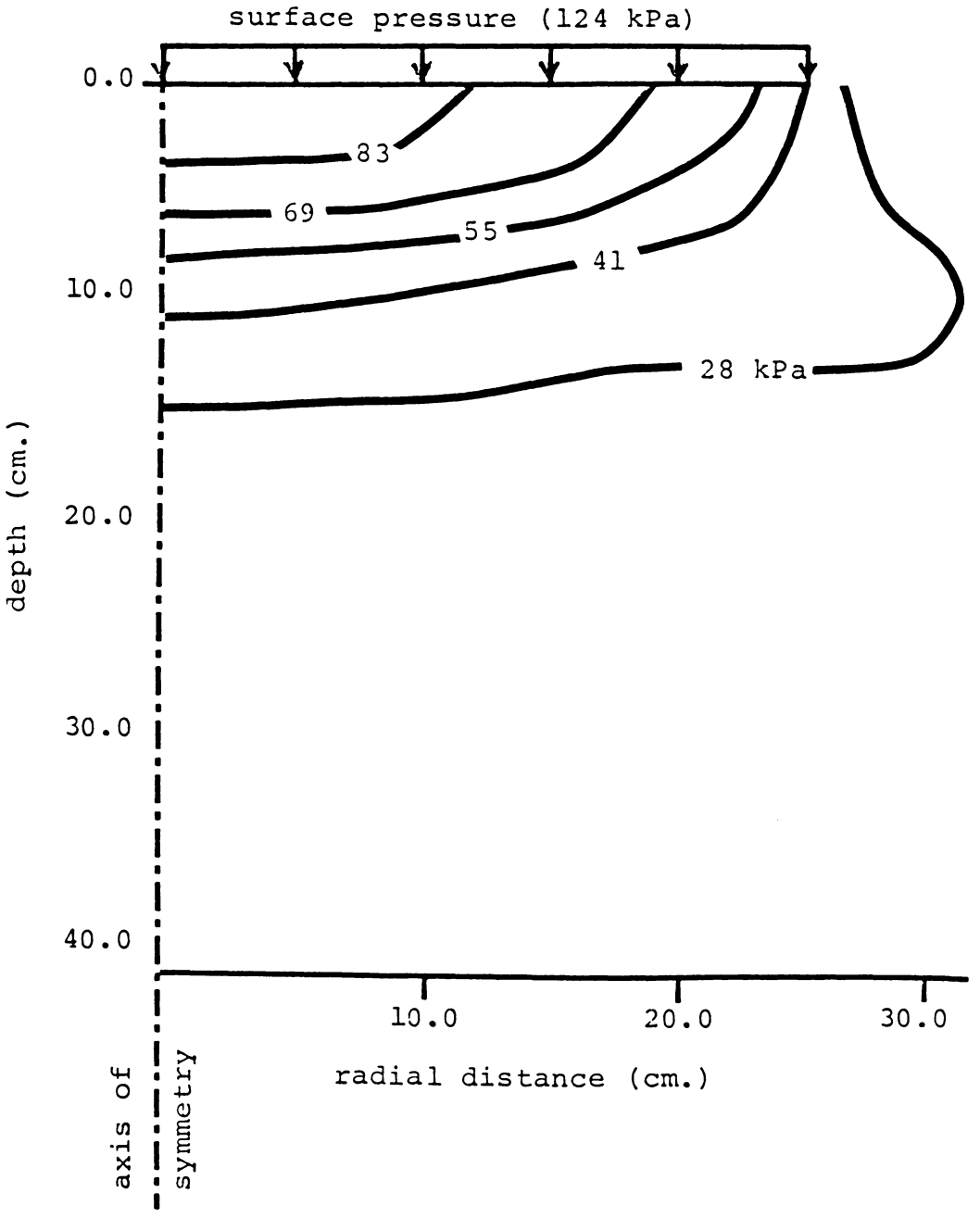

Figure 22: Radial stress bulbs beneath an 18.4-38 bias ply tractor tire in sand.

computing the initial modulus of elasticity (E_i) is considerably higher in sand than in clay, thus indicating a much stiffer soil condition.

Hyperbolic stress-strain curves for elements 157 and 131 are presented in Figures 23 and 24. The maximum deviatoric stress occurs in element 131. The curves are similar to those obtained in the clay soil. However, the magnitude of axial strain in the sand is considerably less than in the clay. This may occur because the value for the parameter n for the sand is comparatively smaller, and magnitudes of ϕ and K are comparatively larger. Analyzing Equation 14, it is evident that this will yield a comparatively larger value for the tangent modulus of elasticity E_t for the sand. This corresponds to a steeper slope on the hyperbolic stress-strain curve (see Figure 2). Thus the magnitude of axial strain in the sand should be smaller than the magnitude of axial strain in the clay at similar levels of deviatoric stress.

Contours of residual volumetric strain obtained from the simulation of five successive wheel loadings on sand are shown in Figures 25 through 29. In this case, the zone of maximum compaction is at the soil surface near the axis of symmetry. This indicates that the depth of maximum soil compaction due to vehicle traffic is dependent upon the

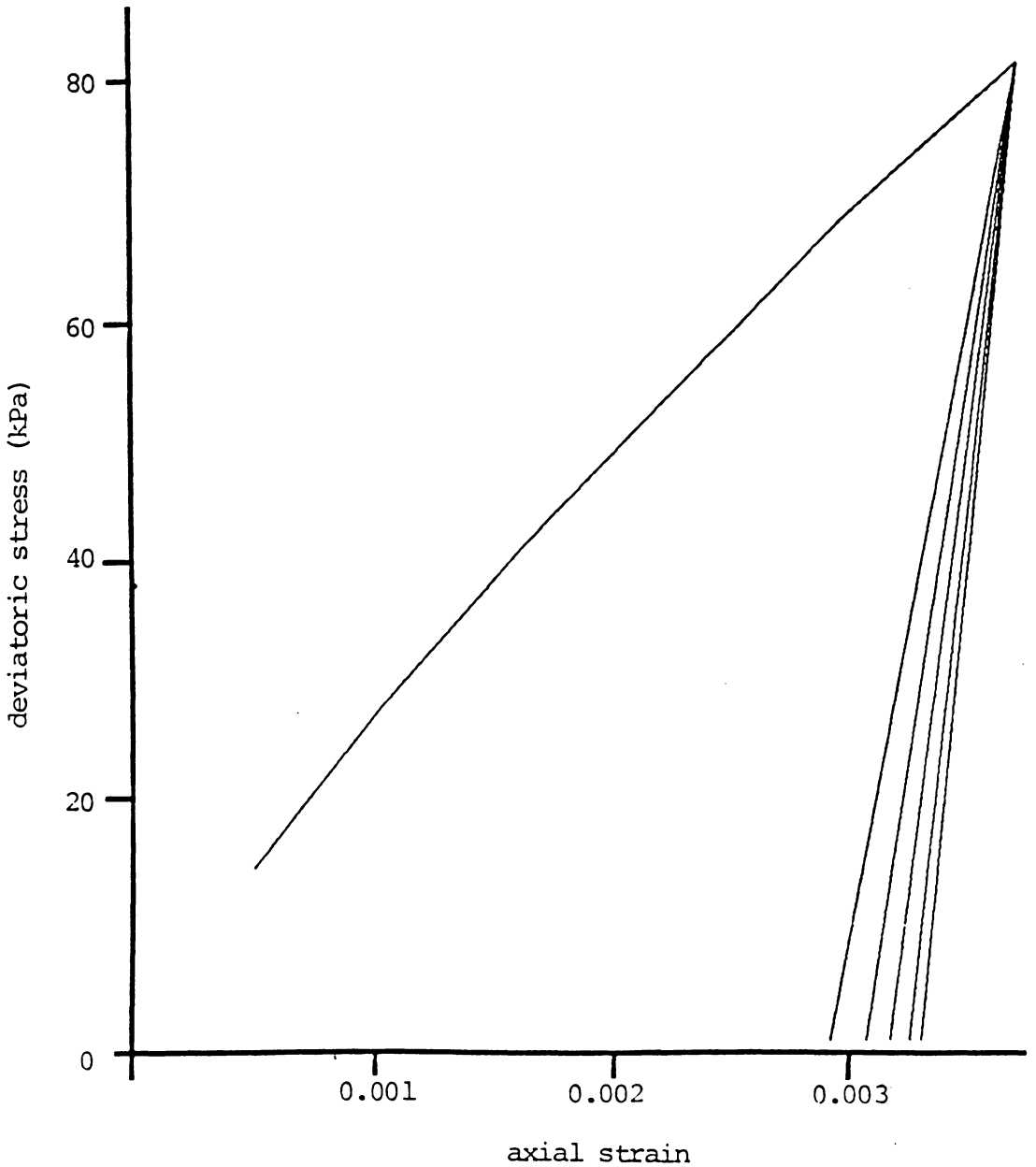

Figure 23: Stress-strain relationship from the results of the finite element analysis for element 131, sandy soil.

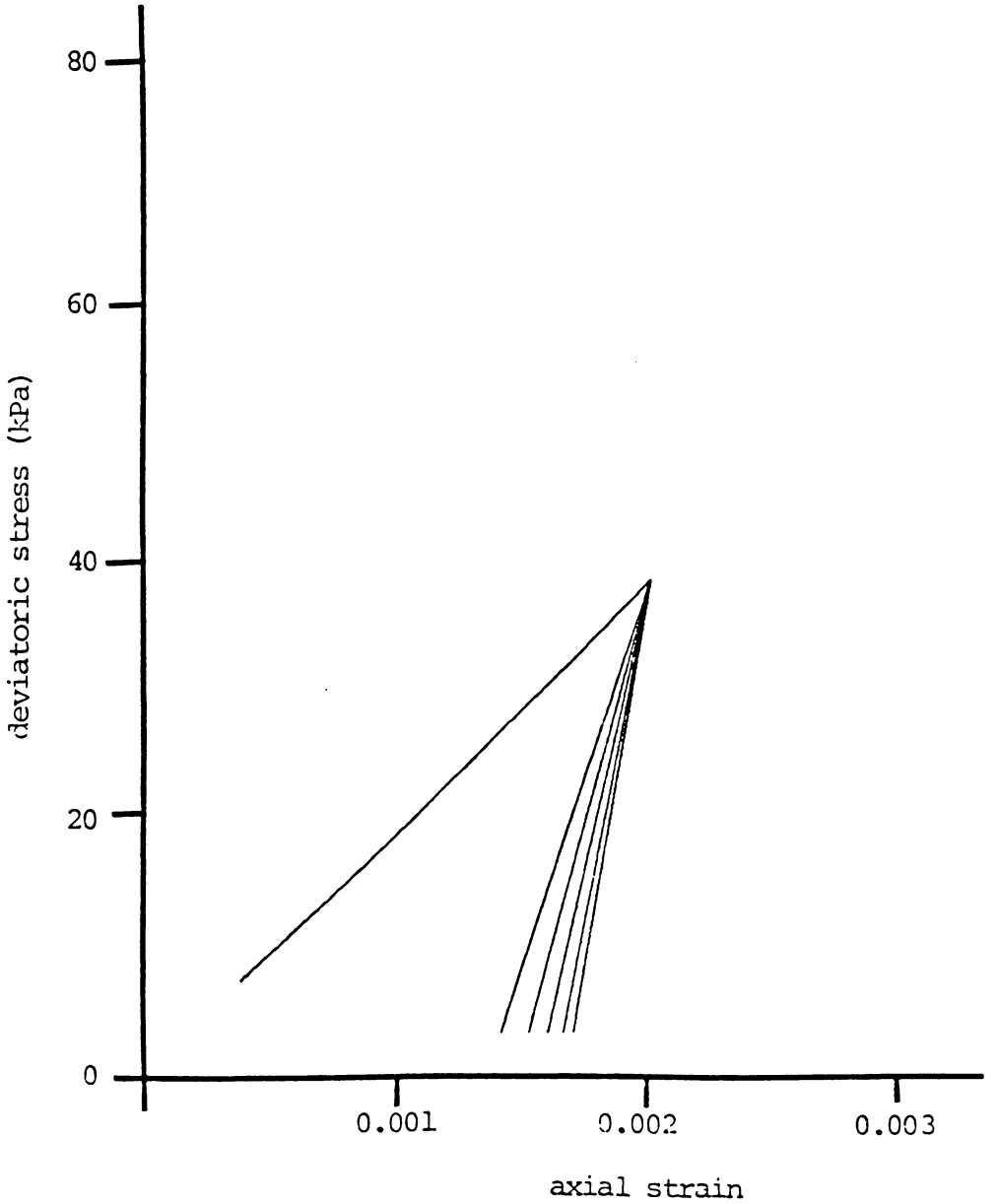

Figure 24: Stress-strain relationship from the results of the finite element analysis for element 157, sandy soil.

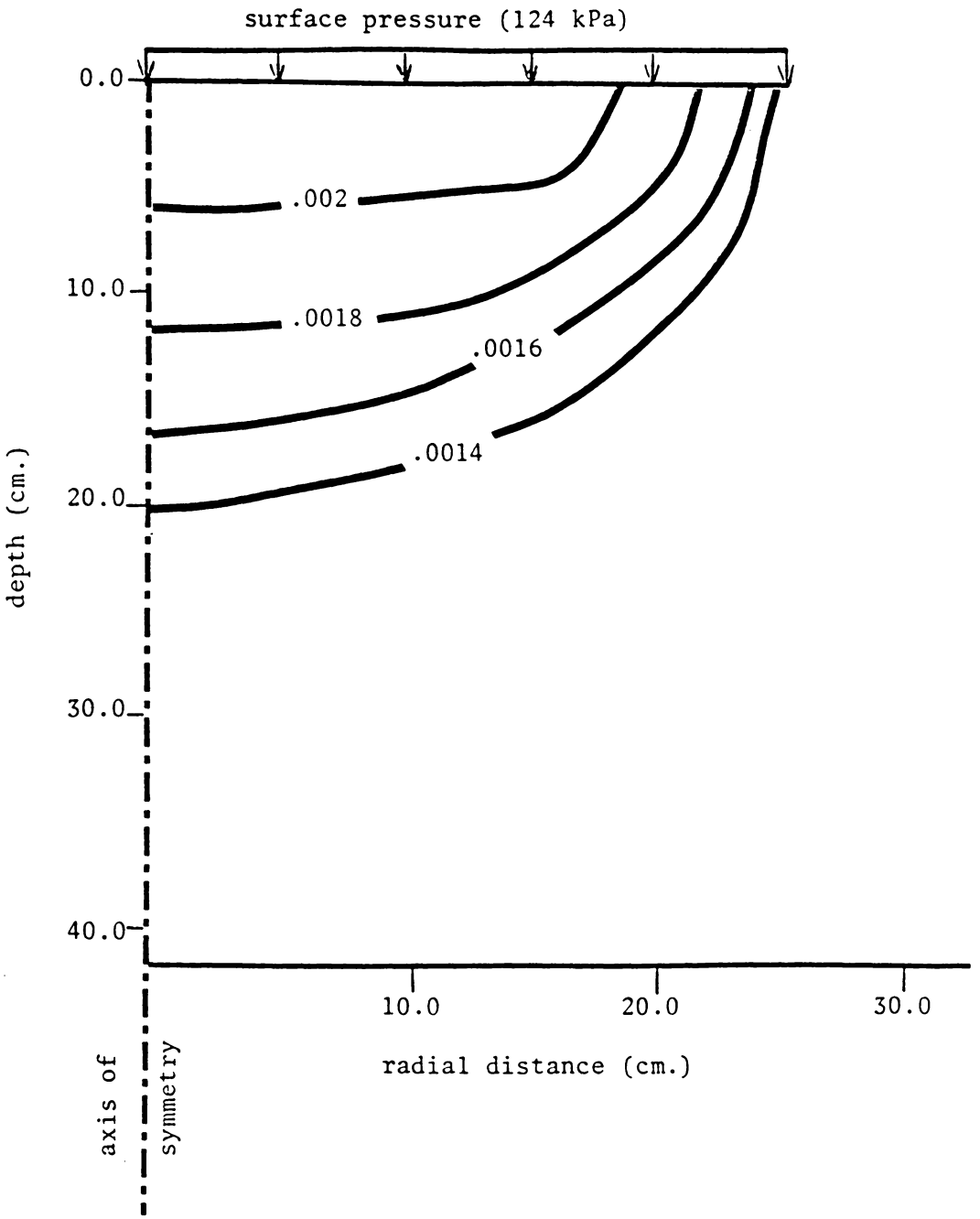

Figure 25: Contours of volumetric strain after one pass of an 18.4-38 bias ply tractor tire in sand.

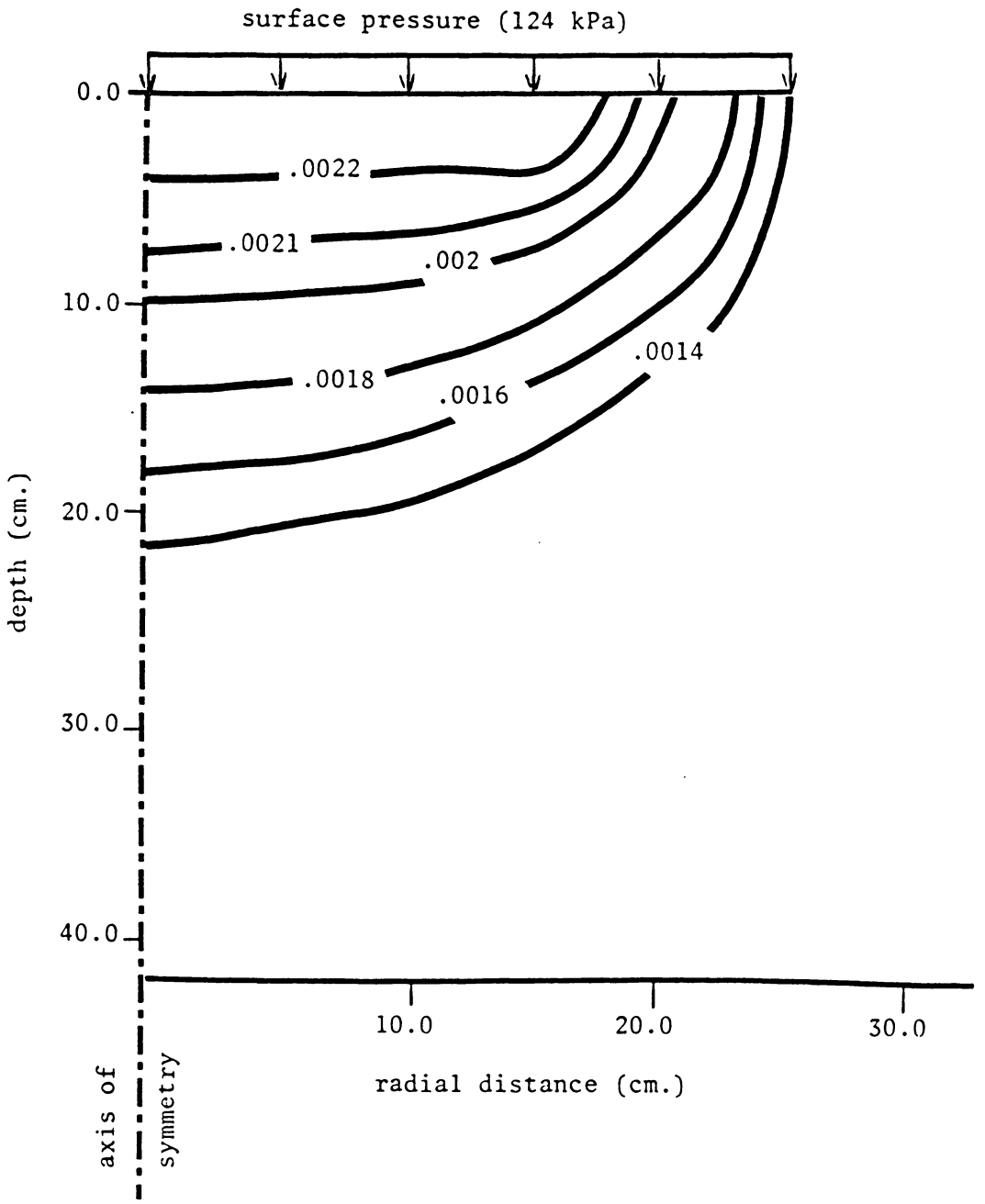

Figure 26: Contours of volumetric strain after two passes of an 18.4-38 bias ply tractor tire in sand.

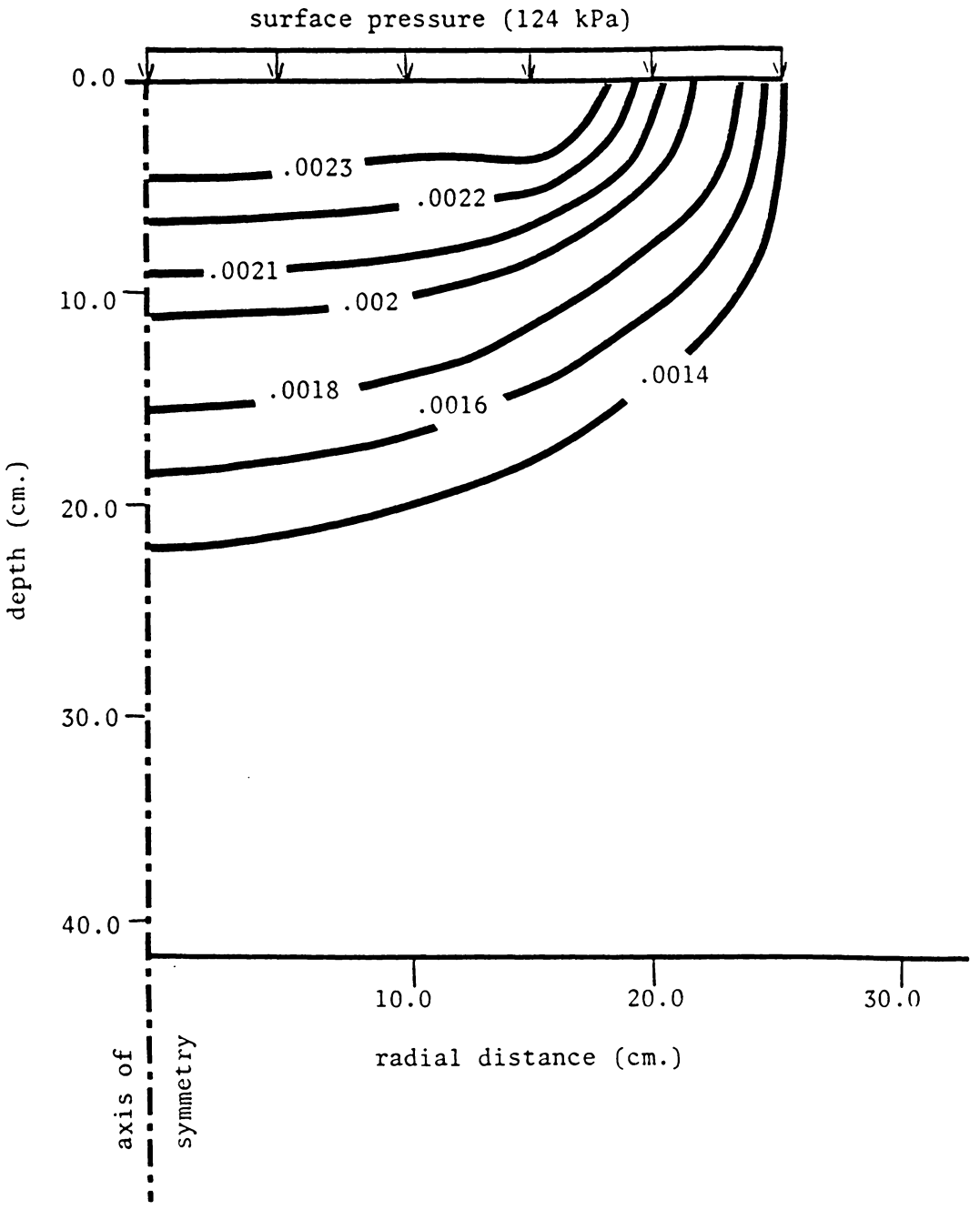

Figure 27: Contours of volumetric strain after three passes of an 18.4-38 bias ply tractor tire in sand.

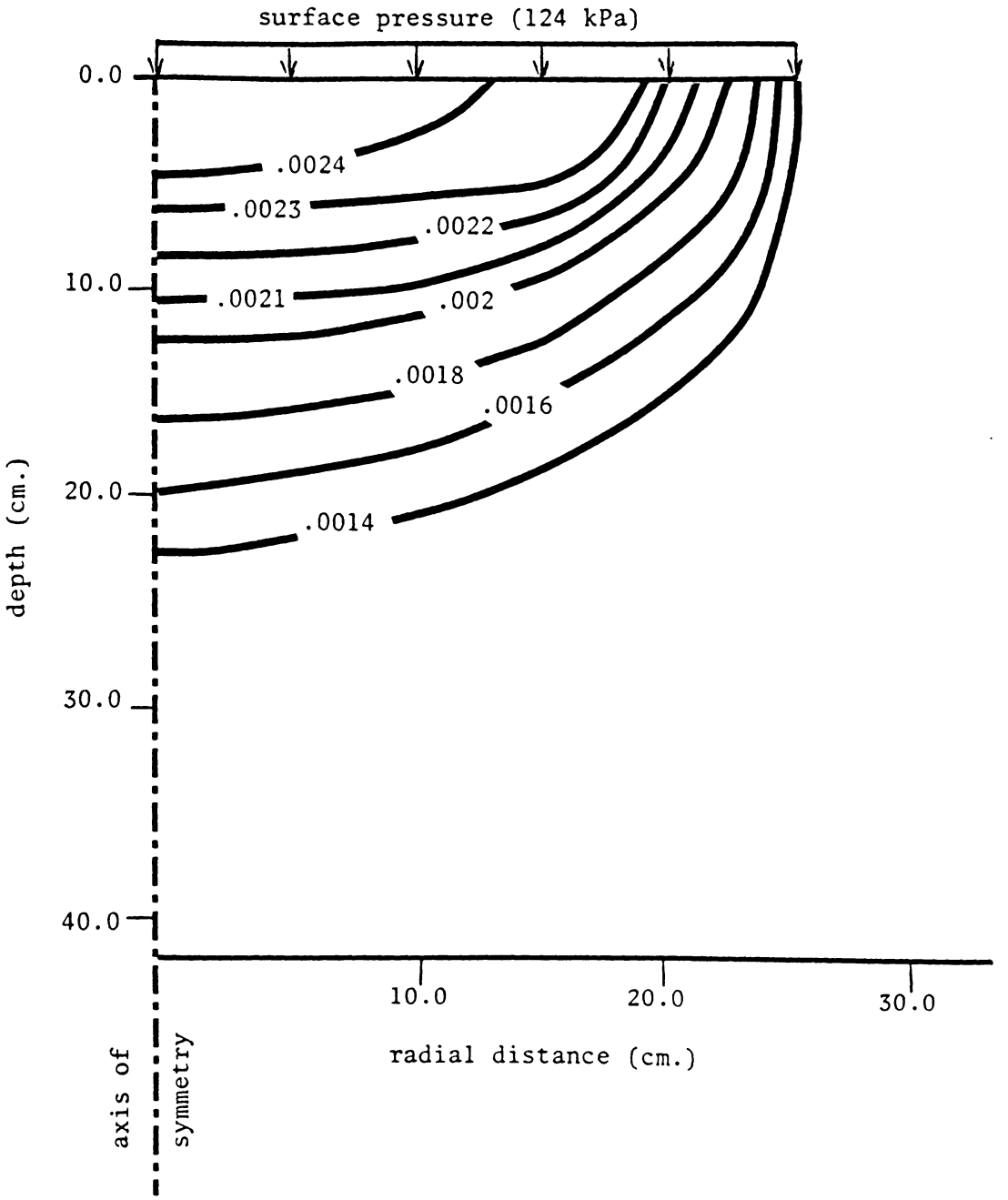

Figure 28: Contours of volumetric strain after four passes of an 18.4-38 bias ply tractor tire in sand.

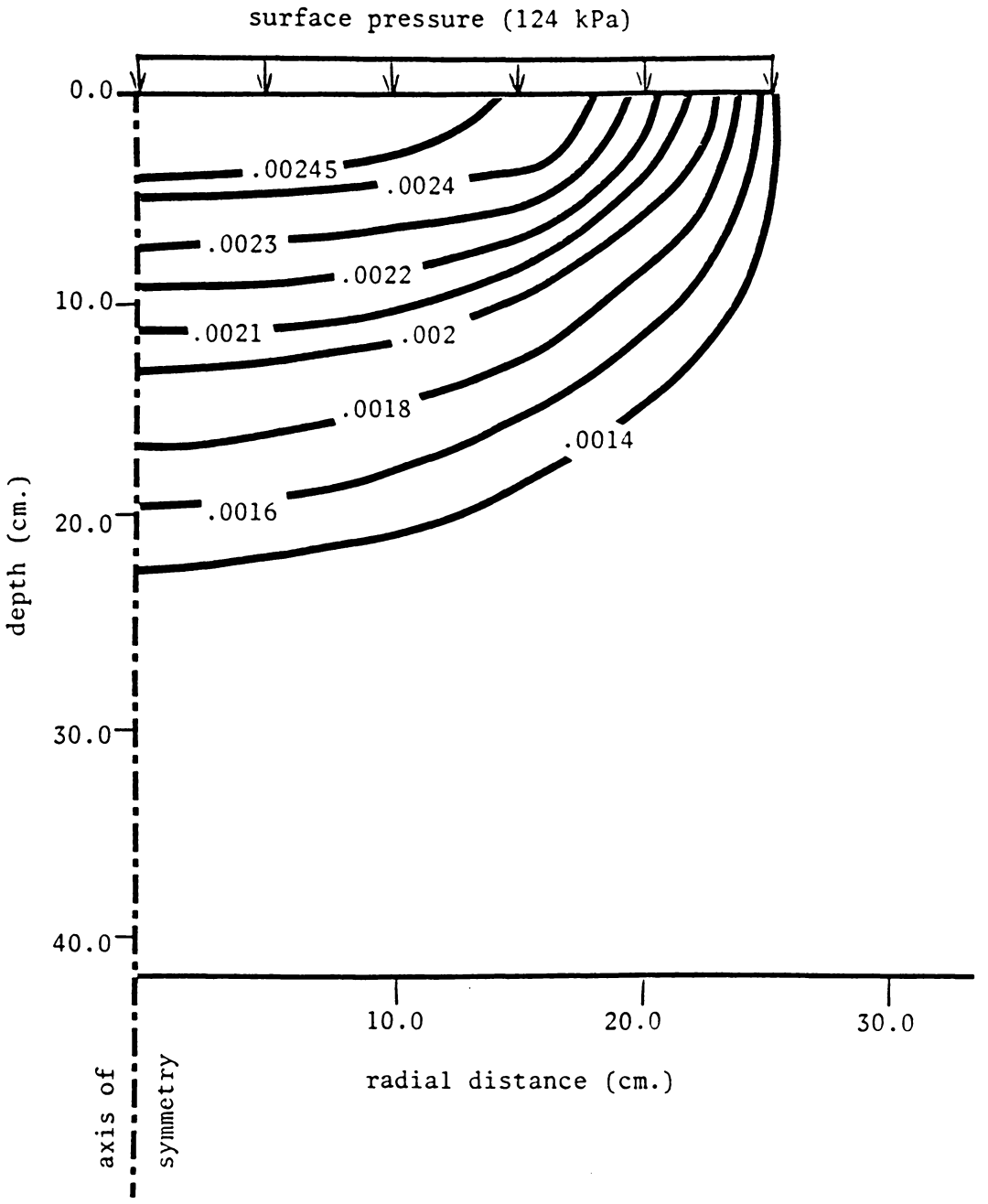

Figure 29: Contours of volumetric strain after five passes of an 18.4-38 bias ply tractor tire in sand.

properties of the soil. The magnitudes of volumetric strain in the sand are considerably less than the magnitudes of volumetric strain in the clay under identical loading conditions. Once again, this is due to the differences in soil properties between the sand and the clay. The growth of strain contours resulting from additional wheel loadings can be observed in Figures 25 through 29.

Figure 30 shows the effect of the number of wheel loadings on volumetric strain for element 157. This element experiences the maximum volumetric strain of 0.00248. This corresponds to an increase in soil bulk density from 1467 kg/m^3 to 1471 kg/m^3. 83.9% of the total volumetric strain occurred during the first wheel loading. The second and third wheel loadings yielded increases in volumetric strain of 6.0% and 4.5%, respectively.

6.4 EFFECT OF TIRE SIZE ON SOIL COMPACTION

The effect of increasing the tire size was simulated by considering the tractor load distributed over a larger contact area in clay. The results of this analysis are compared against those obtained for the 18.4-38 tire in clay. Contours of vertical stress, major principal stress, and radial stress for these conditions are shown in Figures 31, 32, and 33, respectively. The shapes and trends of

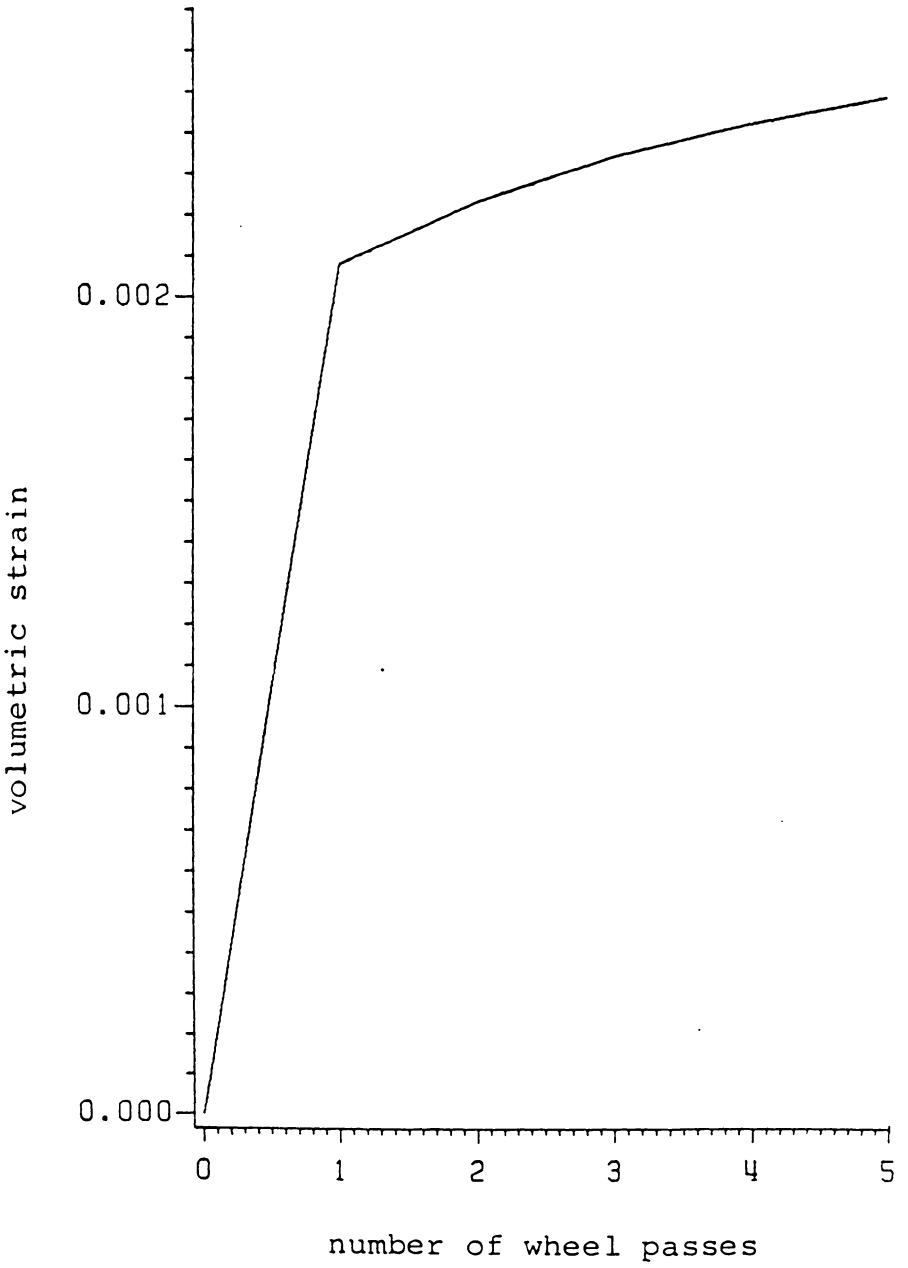

Figure 30: The effect of number of wheel loadings on volumetric strain for element 157 beneath an 18.4-38 bias ply tractor tire in sand.

these stress bulbs are similar to those observed earlier. As expected, the magnitudes of the stress contours are proportionately smaller for the case of a larger wheel.

Contours of residual volumetric strain obtained from the simulation of five successive wheel loadings are shown in Figures 34 through 38. The shapes of these contours are quite different from the contours beneath the 18.4-38 tire in clay and in the case of the larger tire, the soil compaction was found to be maximum at the soil surface. This indicates that for the clay soil, the location of zones of maximum soil compaction depends heavily upon the surface contact area and contact pressure.

The magnitude of volumetric strain for the larger contact area is proportionately smaller. For example, the maximum volumetric strain beneath the 61.0 cm (24.0 in) diameter circular area is only 58.3% of the volumetric strain observed beneath the 18.4-38 bias ply tire (50.8 cm diameter circular area). This observation indicates that the use of wider tires helps to reduce the degree of soil compaction resulting from wheel loading.

Figure 39 shows the effect of the number of wheel loadings on volumetric strain for element 157. This element experienced the maximum volumetric strain of 0.00203, which corresponds to an increase in soil bulk density from 1770

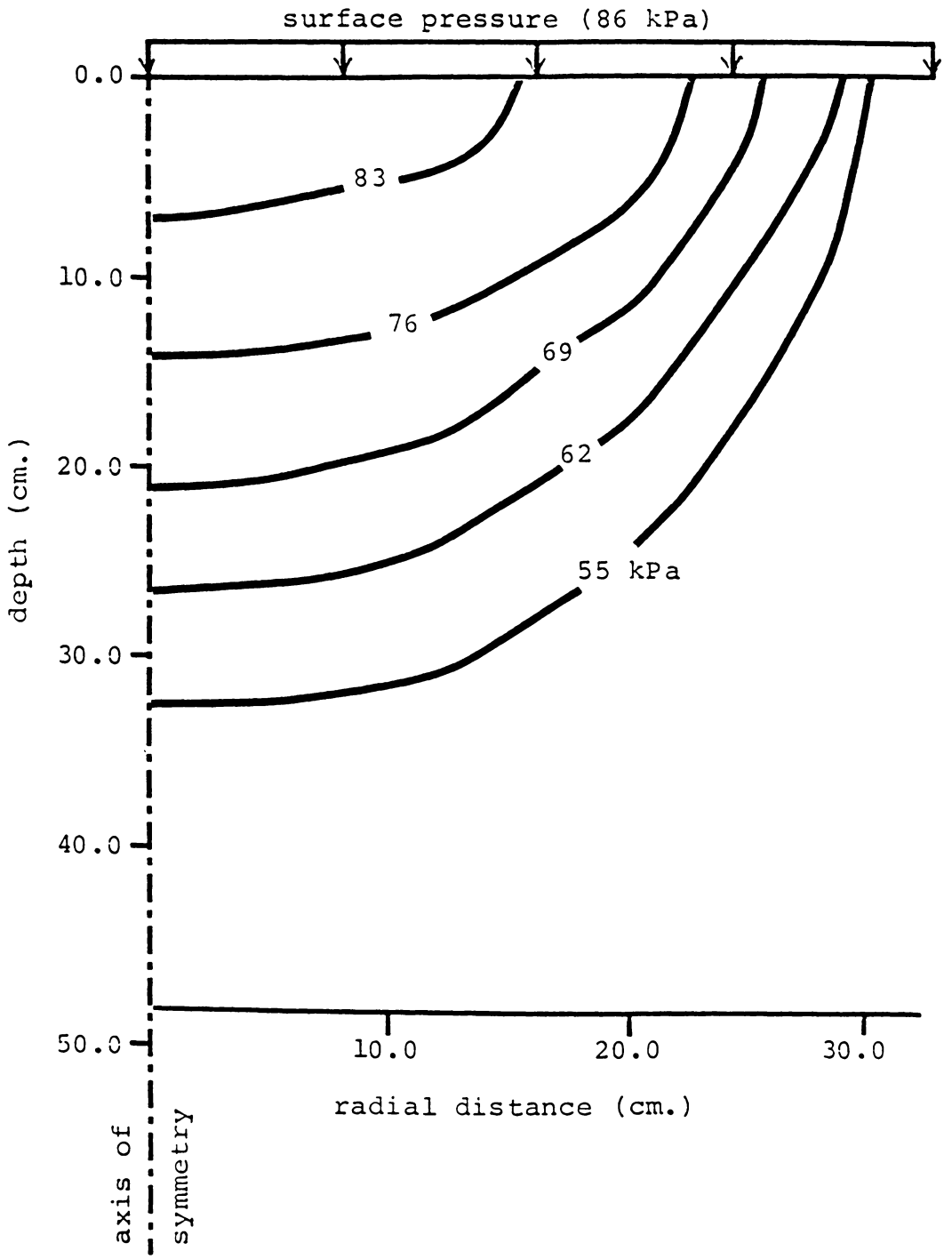

Figure 31: Vertical stress bulbs due to the simulation of a larger tire size in clay.

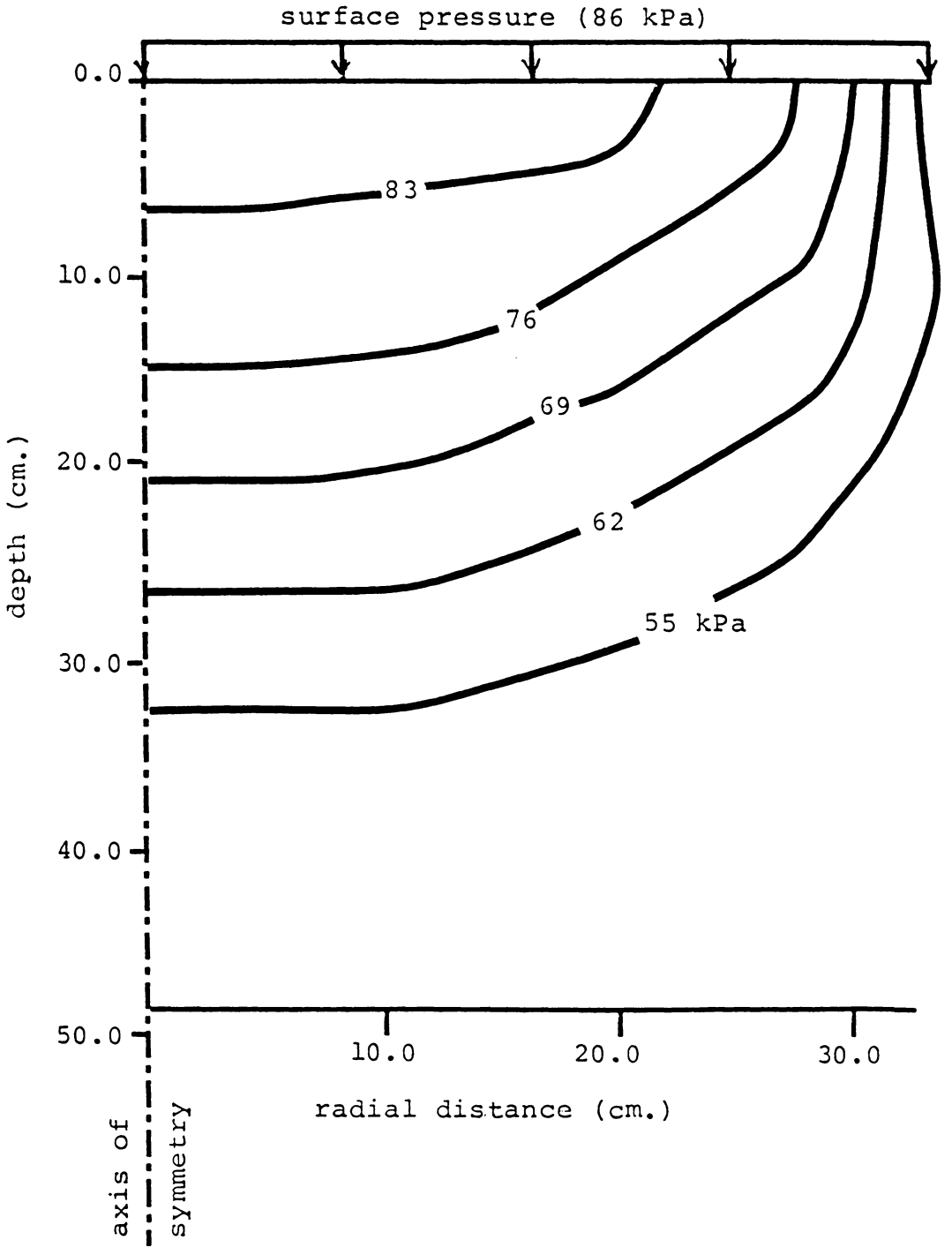

Figure 32: Major principal stress bulbs due to the simulation of a larger tire size in clay.

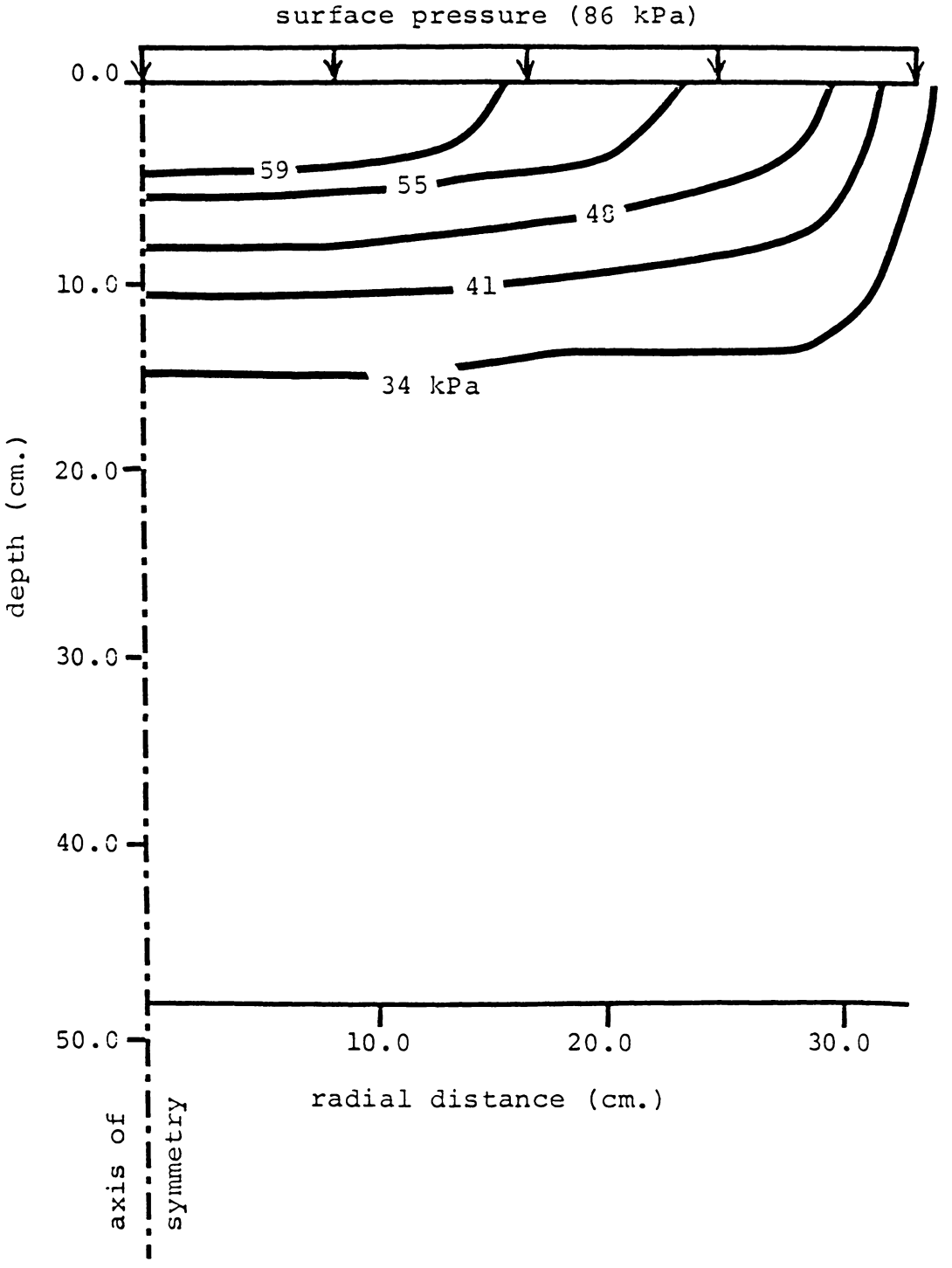

Figure 33: Radial stress bulbs due to the simulation of a larger tire size in clay.

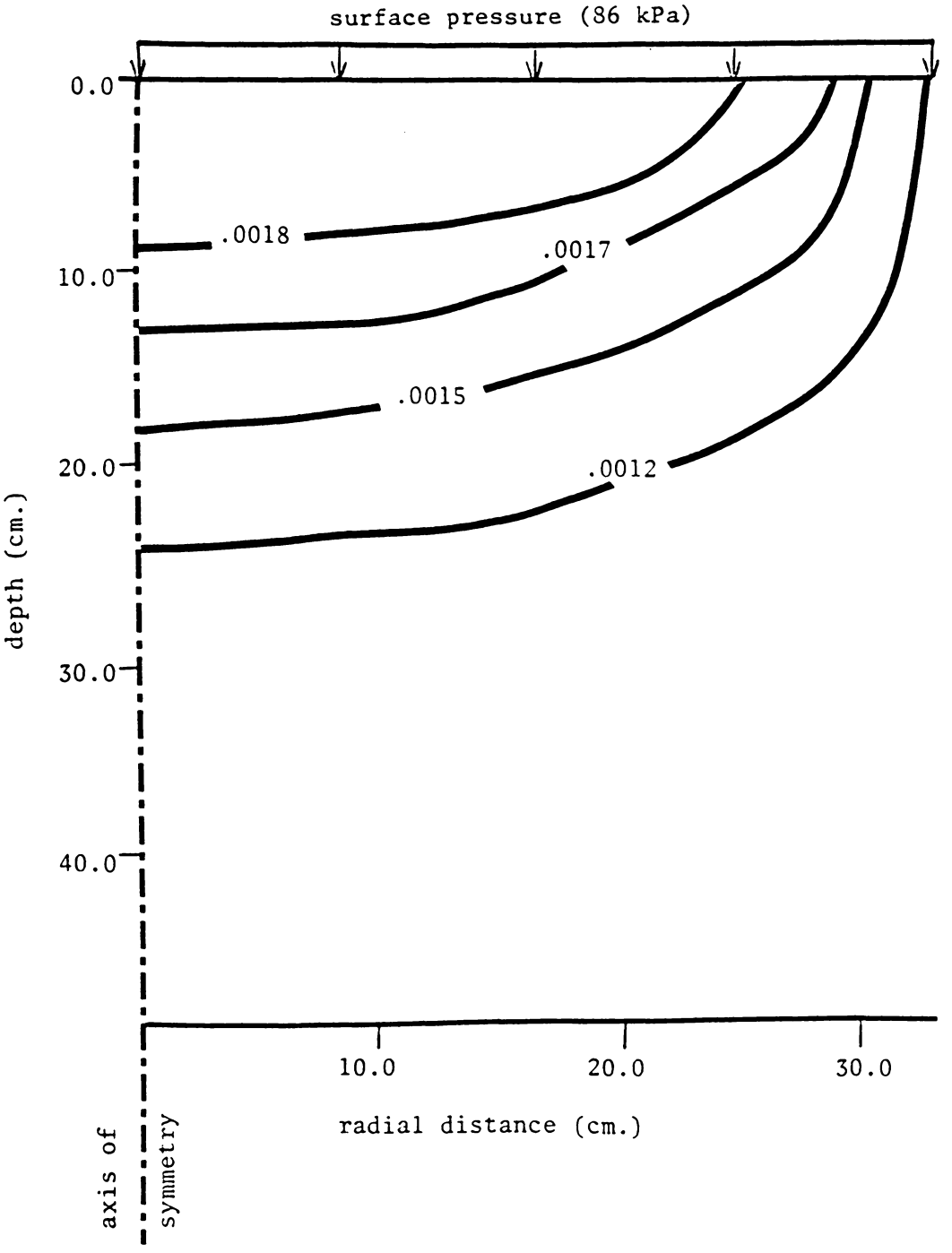

Figure 34: Contours of volumetric strain after one pass of a simulated larger tractor tire in clay.

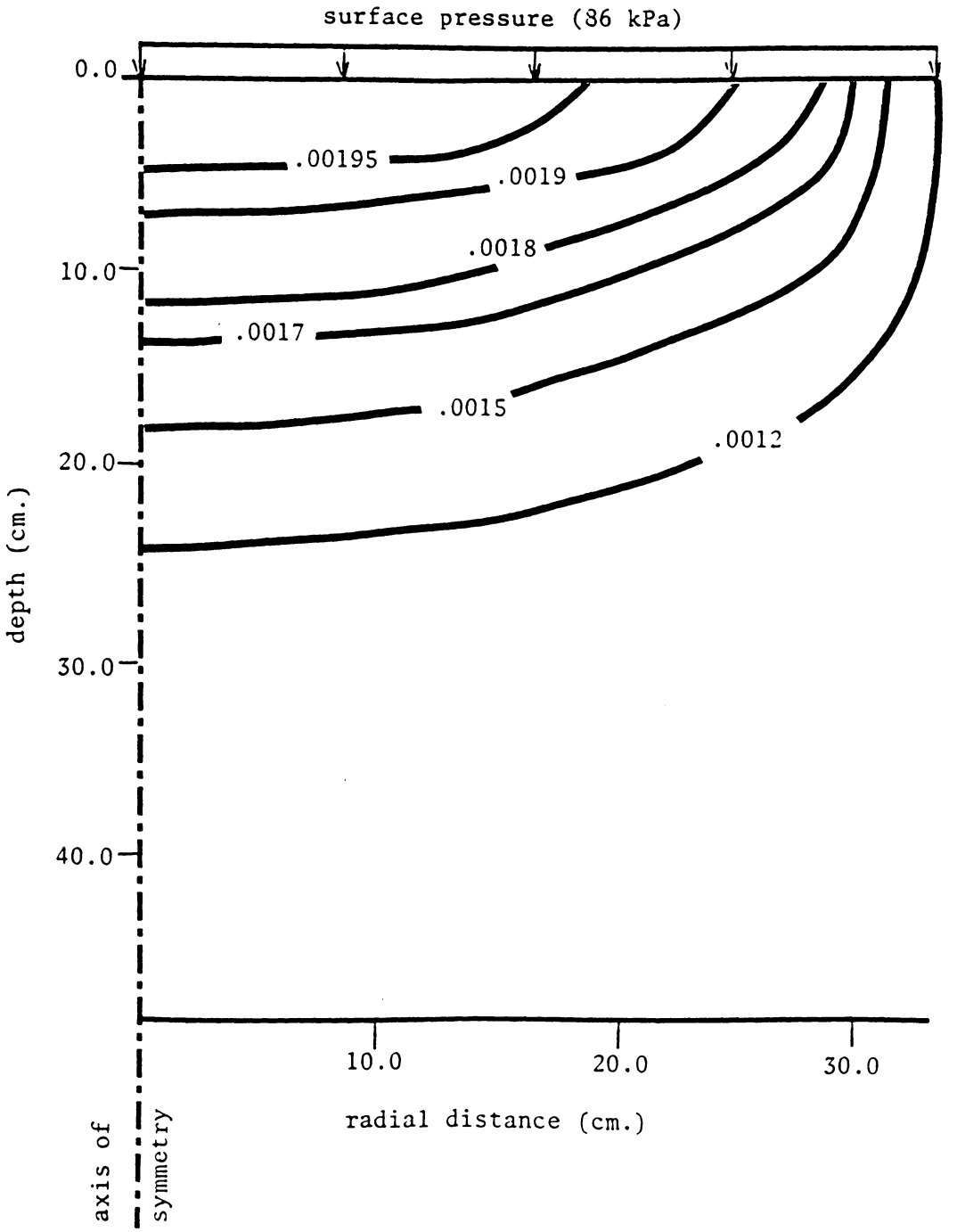

Figure 35: Contours of volumetric strain after two passes of a simulated larger tractor tire in clay.

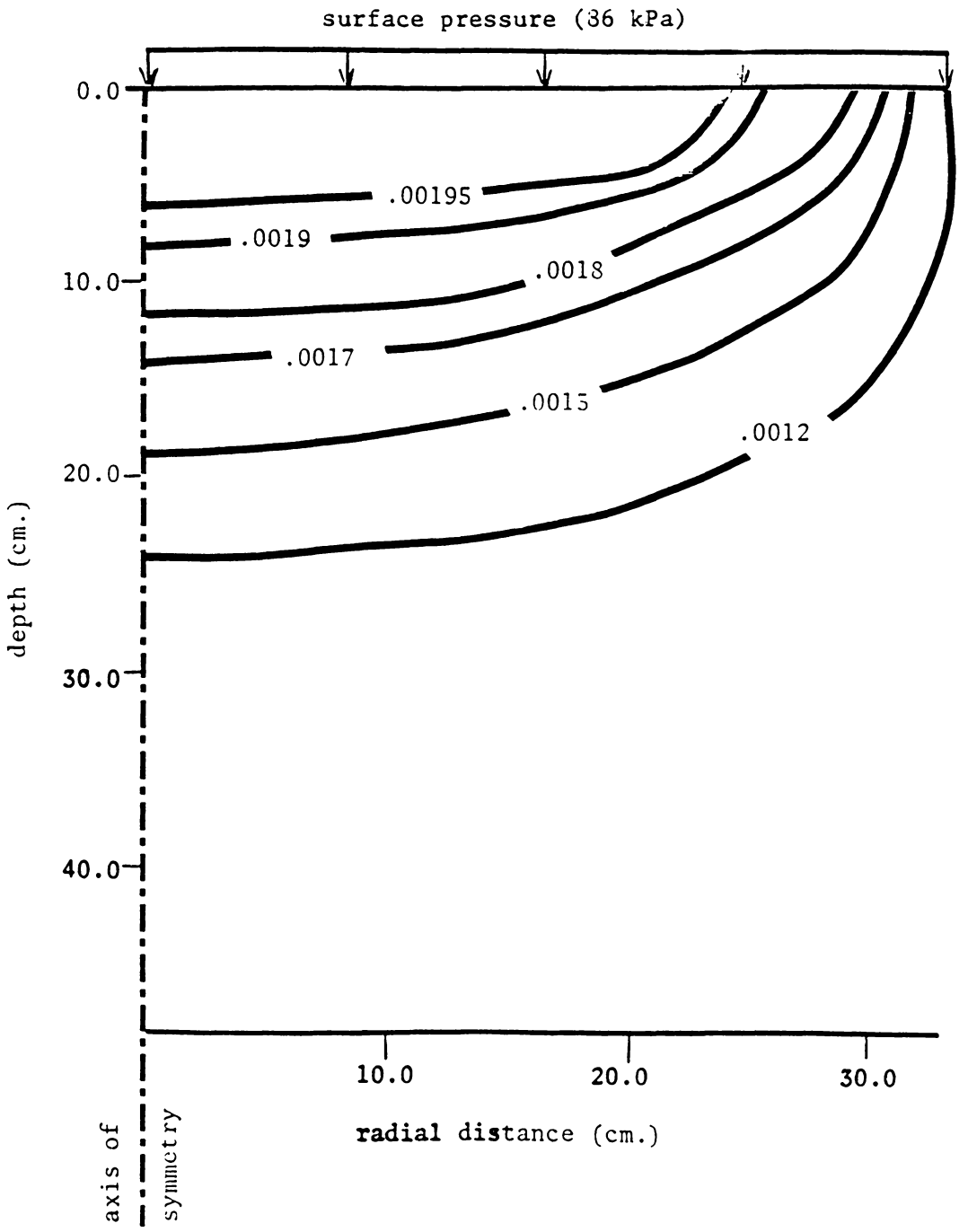

Figure 36: Contours of volumetric strain after three passes of a simulated larger tractor tire in clay.

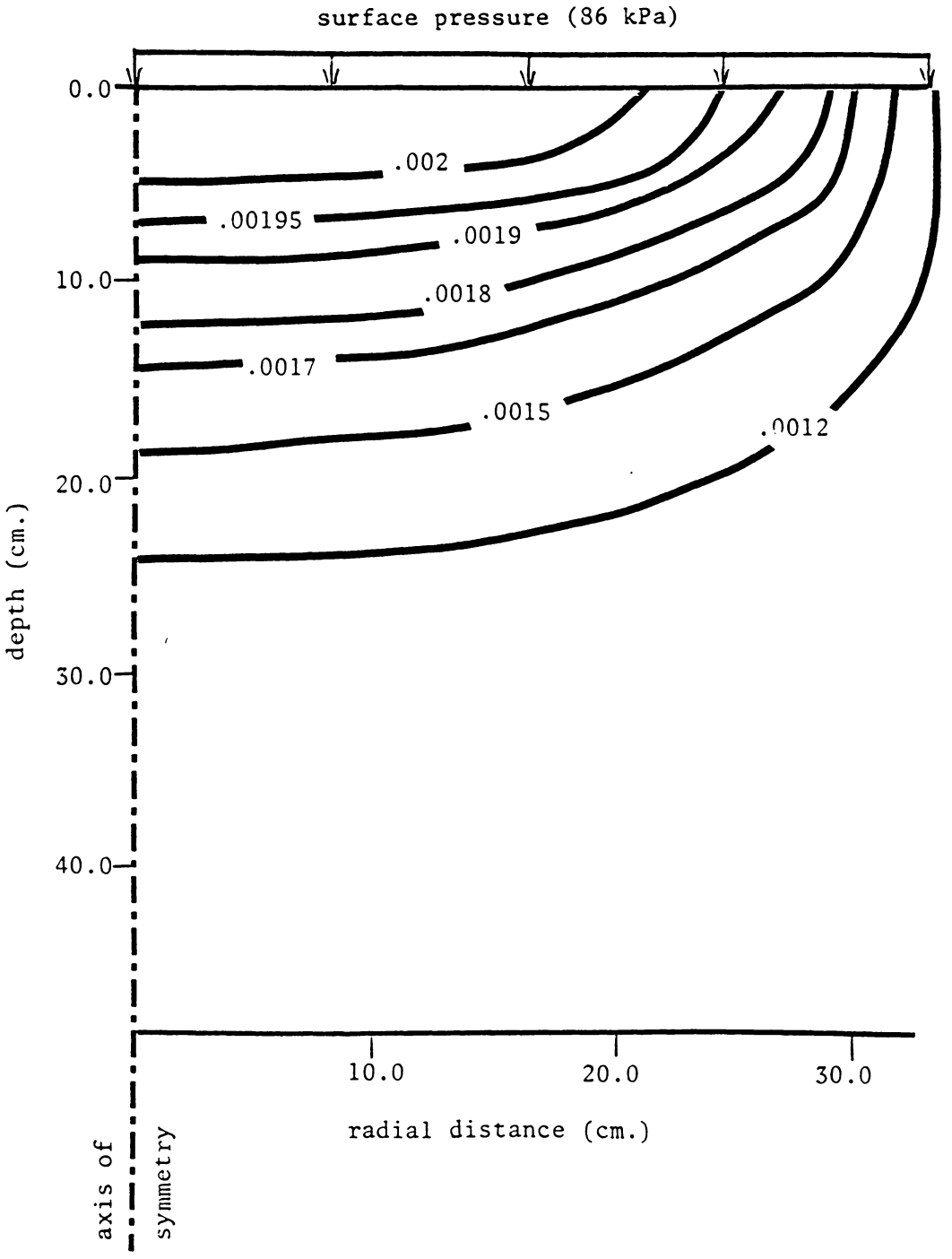

Figure 37: Contours of volumetric strain after four passes of a simulated larger tractor tire in clay.

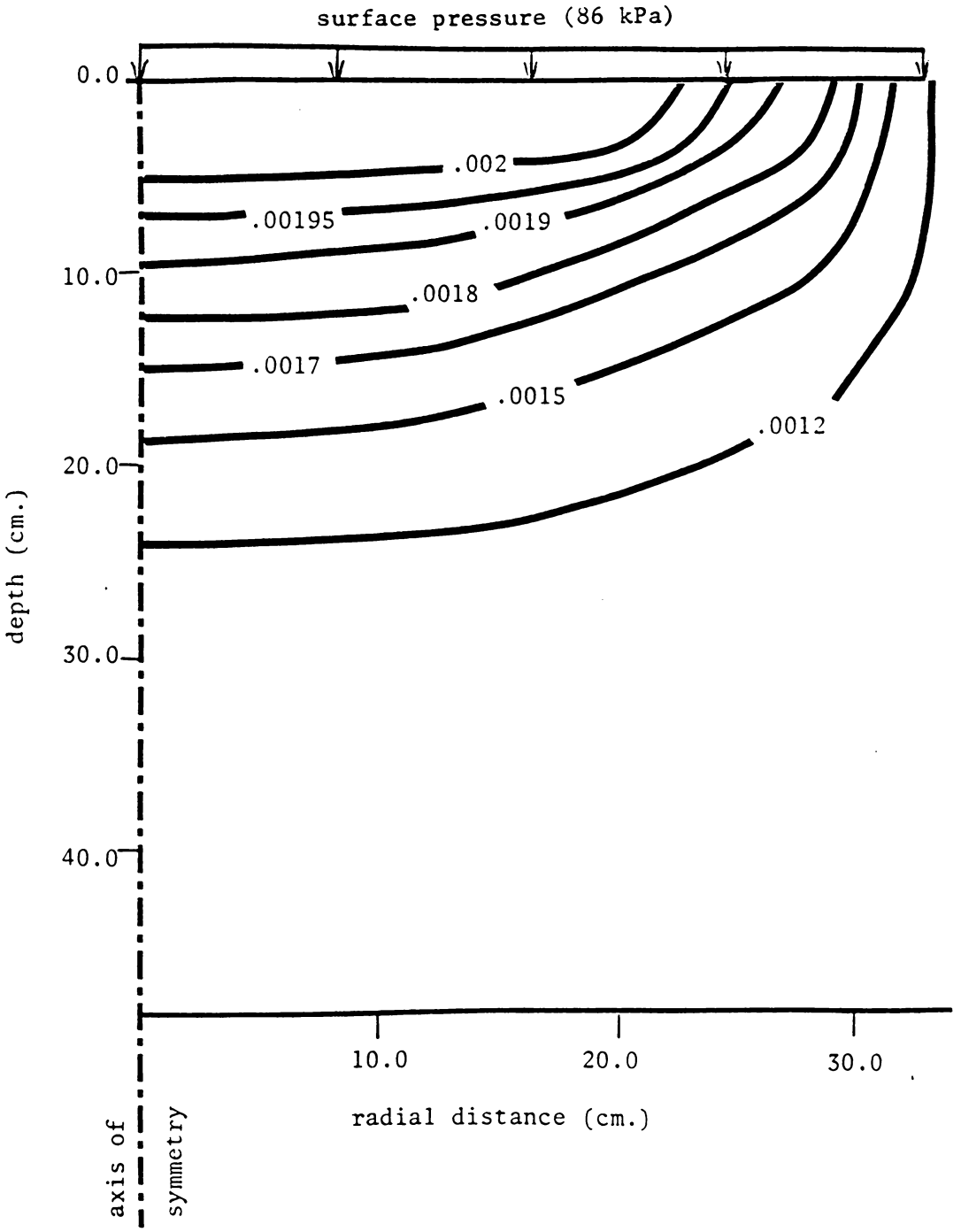

Figure 38: Contours of volumetric strain after five passes of a simulated larger tractor tire in clay.

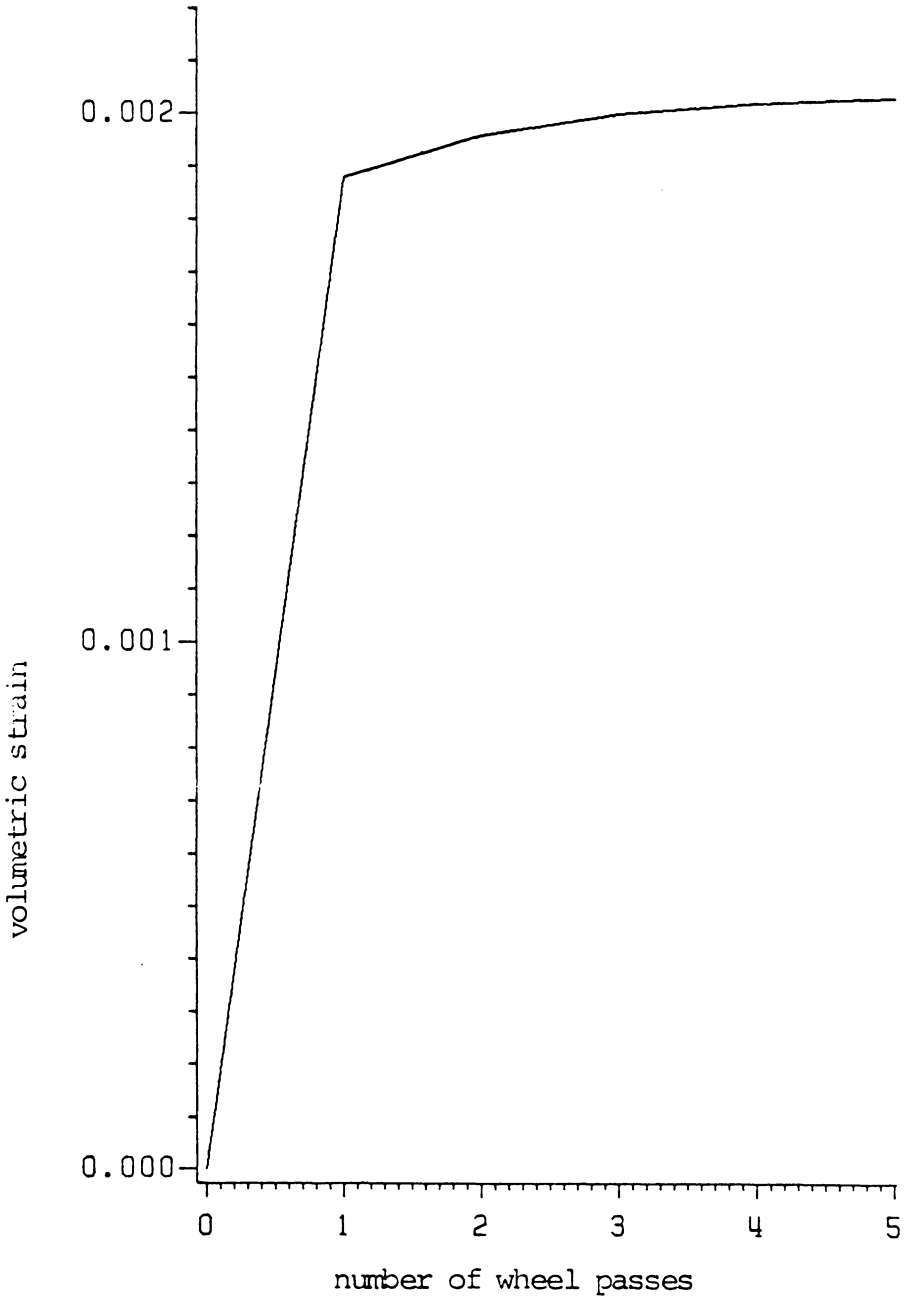

Figure 39: The effect of number of wheel loadings on volumetric strain for element 157 beneath a larger tractor tire in clay.

kg/m^3 to 1774 kg/m^3. 92.6% of the total volumetric strain occurs during the first wheel loading. The second and third wheel loadings yielded increases in volumetric strain of 4.0% and 1.9%, respectively.

A comparison of results from the analysis of an 18.4-38 bias ply tire and a hypothetical larger tire indicated that the tire contact area is an important factor in determining the magnitudes of stress and strain experienced in the clay soil. With a 30.6% increase in tire contact area and the same percentage reduction in contact pressure, the maximum stress and maximum volumetric strain in the soil decreased by 31.0% and 58.3%, respectively. Even though such a comparison was not made in the case of sandy soil, it is reasonable to assume that similar decreases in magnitude of maximum stress and maximum volumetric strain would be observed.

Since the zones of maximum compaction were considerably different for the two contact areas considered, additional analyses were conducted to determine which combination of contact area and contact pressure causes a shift in the maximum compaction zone. The following three combinations of contact area and contact pressure were considered:

1. A 112 kPa (16.3 psi) surface pressure uniformly distributed over a 53.3 cm (21.0 in) diameter circular area.

2. A 103 kPa (14.9 psi) surface pressure uniformly distributed over a 55.9 cm (22.0 in) diameter circular area.
3. A 93.8 kPa (13.6 psi) surface pressure uniformly distributed over a 58.4 cm (23.0 in) diameter circular area.

A comparison of the results of these analyses showed that the zone of maximum soil compaction shifted from within the soil to the soil surface, directly beneath the loaded area when the diameter of the loaded area was increased from 53.3 cm to 55.9 cm. The reason for this shift in the zone of maximum compaction is not known, and further study is needed to better understand this behavior.

Chapter VII

CONCLUSIONS

The finite element analysis of soil compaction due to multiple wheel loading has led to the following conclusions:

1. The finite element method can be used to locate the zones of maximum compaction and to illustrate the propogation of compaction zones due to multiple wheel loading.
2. The effect of soil type and soil condition on compaction can be observed by developing appropriate constitutive relationships for soils of interest.
3. The model developed can be used to demonstrate the effect of tire size on soil compaction. An increase in contact area yielded a decrease in the magnitude of maximum stress and volumetric strain within the soil profile.
4. Results of the finite element analysis demonstrated that the major portion of permanent compaction occurred during the first wheel loading. Successive wheel loadings yielded relatively smaller increases in compaction.

BIBLIOGRAPHY

Bailey, Alvin C. 1971. Compaction and shear in compacted soils. Transactions of the ASAE, 14(2): 201-205.

Bailey, Alvin C. and G. E. VandenBerg. 1968. Yielding by compaction and shear in unsaturated soils. Transactions of the ASAE, 11(3): 307-311,317.

Bergmann, E. P. 1979. Compaction. Journal of Terramechanics, 16(1): 23-32.

Bodman, G. B. and J. Rubin. 1948. Soil puddling. Proceedings of the Soil Science Society of America, 13: 27-36.

Brooker, E. W. and H. O. Ireland. 1965. Earth pressures at rest related to stress history. Canadian Geotechnical Journal, 2(1): 1-15.

Chancellor, W. J., R. H. Schmidt, and W. H. Soehne. 1962. Laboratory measurement of soil compaction and plastic flow. Transactions of the ASAE, 5(2): 235-239.

Clough, Ray W. and Richard J. Woodward. 1967. Analysis of embankment stresses and deformations. Journal of the Soil Mechanics and Foundations Division, Proceedings of the ASCE, 93(4): 529-549.

Desai, Chandrakant S. Elementary Finite Element Method. Prentice-Hall,Inc., Englewood Cliffs, NJ, 1979.

Desai, Chandrakant S. and John F. Abel. Introduction to the Finite Element Method. Van Nostrand Reinhold Company, New York, NY, 1972.

Duncan, James M. and Chin-Yung Chang. 1970. Nonlinear analysis of stress and strain in soils. Journal of the Soil Mechanics and Foundations Division, Proceedings of the ASCE, 96(5): 1629-1653.

Froehlich, Henry A., J. Azevedo, Peter Cafferata, and Dave Lysne. 1980. Predicting soil compaction on forested land. Final Project Report to U.S. Forest Service, Forest Engineering Dept., Oregon State University.

Gill, William R. and Carl A. Reaves. 1956. Compaction patterns of smooth rubber tires. Agricultural Engineering, 37: 677-680,684.

Girijavallabhan, C. V. and L. C. Reese. 1968. Finite element method for problems in soil mechanics. Journal of the Soil Mechanics and Foundations Division, Proceedings of the ASCE, 94(2): 473-496.

Harr, M. E. Foundations of Theoretical Soil Mechanics. McGraw-Hill Book Company, 1966.

Harris, W. L., W. F. Buchele, and L. E. Malvern. 1964. Relationship of mean stress, volumetric strain and dynamic loads in soil. Transactions of the ASAE, 7(4): 362-364,369.

Hettiaratchi, D. R. P. and J. R. O'Callaghan. 1980. Mechanical behaviour of agricultural soils. Journal of Agricultural Engineering Research, 25:239-259.

Jaafari, Hamid and Henry D. Bowen. 1980. Limitation of Boussinesq's equation for simulating wheel compaction. ASAE Paper No. 80-1517.

Jumikis, A. R. Soil Mechanics. Edited by S. F. Borg. D. Van Nostrand Company,Inc., New York, NY, 1962.

King, A. L. 1979. Measuring soil compaction in mechanically thinned pine plantations. ASAE Paper No. 79-1600.

Kulhawy, F. H., J. M. Duncan, and H. B. Seed. 1969. Finite element analysis of stresses and movements in embankments during construction. Contract Report No. TE-69-4, USAEWES.

Minaei, Saeid. 1983. The effect of track and rubber tired vehicles on soil compaction. Unpublished thesis. Virginia Polytechnic Institute and State University.

Negi, S. C., E. McKyes, G. S. V. Raghavan, and F. Taylor. 1981. Relationships of field traffic and tillage to corn yields and soil properties. Journal of Terramechanics, 18(2): 81-90.

Onafeko, O. and A. R. Reece. 1967. Soil stress and deformation beneath rigid wheels. Journal of Terramechanics, 4(1): 59-80.

Perumpral, J. V. 1969. The finite element method for predicting stress distribution and soil deformation under a tractive device. Ph.D. Thesis, Purdue University.

Perumpral, J. V. and T. Kuppusamy. 1983. Finite element modeling of soil-machine problems. SAE Technical Paper Series, Paper No. 830806.

Perumpral, J. V., J. B. Liljedahl, and W. H. Perloff. 1971. The finite element method for predicting stress distribution and soil deformation under a tractive device. Transactions of the ASAE, 14(6): 1184-1188.

Poulos, H. G. and E. H. Davis. Elastic Solutions for Soil and Rock Mechanics. John Wiley and Sons,Inc., New York, NY, 1974.

Raghavan, G. S. V. and E. McKyes. 1978. Statistical models for predicting compaction generated by off-road vehicular traffic in different soil types. Journal of Terramechanics, 15(1): 1-14.

Raghavan, G. S. V., E. McKyes, and M. Chasse. 1977. Effect of wheel slip on soil compaction. Journal of Agricultural Engineering Research, 22: 79-83.

Soehne, Walter. 1958. Fundamentals of pressure distribution and soil compaction under tractor tires. Agricultural Engineering, 39: 276-281,290.

Stafford, J. V. and P. de Carvalho Mattos. 1981. The effect of forward speed on wheel-induced soil compaction: laboratory simulation and field experiments. Journal of Agricultural Engineering Research, 26: 333-347.

Taylor, James H., Eddie C. Burt, and Alvin C. Bailey. 1978. Traction and compaction of big tractors. ASAE Paper No. 78-1029.

Taylor, James H., Albert C. Trouse, Jr., Eddie C. Burt, and Alvin C. Bailey. 1979. Multipass behavior of a pneumatic tire on tilled soils. ASAE Paper No. 79-1549.

Threadgill, E. Dale. 1982. Residual tillage effects as determined by cone index. Transactions of the ASAE, 25(1): 859-863, 867.

Turner, John L. 1982. A semiempirical mobility model for tracked skidders. ASAE Paper No. 82-1597.

VandenBerg, G. E. 1966. Triaxial measurements of shear strain and compaction in unsaturated soil. Transactions of the ASAE, 9(4): 460-463,467.

VandenBerg, G. E., W. F. Buchele, and L. E. Malvern. 1958. Applications of continuum mechanics to soil compaction. Transactions of the ASAE, 1(1): 24-27.

Yong, R. N. and E. A. Fattah. 1976. Prediction of wheel-soil interaction and performance using the finite element method. Journal of Terramechanics, 13(4): 227-240.

Yong, R. N., E. A. Fattah, and P. Boonsinsuk. 1978. Analysis and prediction of tyre-soil interaction and performance using finite elements. Journal of Terramechanics, 15(1): 43-63.

Yong, R. N. and A. W. Hanna. 1977. Finite element analysis of plane soil cutting. Journal of Terramechanics, 14(3): 103-125.

Zienkiewicz, D. C. The Finite Element Method in Engineering Science. McGraw-Hill, London, 1971.

The vita has been removed from the scanned document